UCRL-2956
Unclassified Physics

UNIVERSITY OF CALIFORNIA

Radiation Laboratory
Berkeley, California

Contract No. W-7405-eng-48

PHOTODISINTEGRATION OF DEUTERONS AT HIGH ENERGIES

Dwight R. Dixon

(Thesis)

March 30, 1955

CERN LIBRARIES, GENEVA

Printed for the U. S. Atomic Energy Commission

PHOTODISINTEGRATION OF DEUTERONS AT HIGH ENERGIES

Contents

PHOTODISINTEGRATION OF DEUTERONS AT HIGH ENERGIES

Dwight R. Dixon

Radiation Laboratory and Department of Physics
University of California, Berkeley, California

March 30, 1955

ABSTRACT

Photodisintegration of deuterons has been investigated by use of the photon beam from the 335-Mev synchrotron at Berkeley. A liquid deuterium target was used. Protons were detected with a telescope consisting of either twelve or thirteen scintillation counters. Pulses from these counters were presented on an oscilloscope and recorded photographically. The height of the pulse from one of the first counters and the number of subsequent pulses served to identify the protons and determine their energy.

Differential cross sections were determined at laboratory angles of 36°, 49°, 75°, 106°, and 141° and at energies ranging from 136 Mev to 293 Mev, and curves of the form $d\sigma/d\Omega' = A + B \cos \theta' + C \cos^2 \theta'$ were fitted to the experimental points at various energies. The ratio B/A decreased from 0.46 at 143 Mev to 0.16 at 293 Mev. The ratio C/A was of the order of -0.4. Total cross sections of about 70 μb were obtained and there was some indication of a maximum in the total cross section in the vicinity of 250 Mev.

A comparison is made with the results of similar experiments at other laboratories. Some suggested interpretations of the observed results are discussed briefly.

PHOTODISINTEGRATION OF DEUTERONS AT HIGH ENERGIES

Dwight R. Dixon

Radiation Laboratory and Department of Physics
University of California, Berkeley, California

March 30, 1955

I. INTRODUCTION

One of the most fruitful sources of knowledge of the nature of nuclear forces has been the study of problems in which only two nucleons are involved. Examples of two-body problems are the ground state of the deuteron, nucleon-nucleon scattering, and photodisintegration of the deuteron. Because of the relative simplicity of these systems one might hope to interpret the experimental results theoretically and thus obtain parameters relating to the nuclear forces.

Photodisintegration of deuterons was first accomplished by Chadwick and Goldhaber[1] in 1934, using 2.62-Mev gamma rays. The problem was first considered theoretically by Bethe and Peierls.[2] Experimental and theoretical studies in the low-energy region are described by Ramsey,[3] Squires,[4] and Blatt and Weisskopf.[5] In the region just above threshold the magnetic dipole photoeffect predominates. This effect becomes negligible a few Mev above threshold and the electric dipole interaction becomes the predominant one. By considering these interactions and introducing the effective range theory of nuclear forces, one can obtain a satisfactory fit to the experimental data up to about 10 Mev. The shape of the nuclear potential well has no appreciable effect on the cross sections.

In calculating the electric dipole transition probabilities above 10 Mev it becomes necessary to consider the detailed nature of nuclear forces. The nature of the wave function inside the range of the nuclear

force becomes important. The phase shift in the final state, which was neglected in lower-energy calculations, must be considered, and it depends on the exchange nature of the neutron-proton force. Also at energies above 10 Mev it is no longer possible to neglect quadrupole transitions. Calculations involving these considerations are discussed briefly by Blatt and Weisskopf.[5] Calculations of the deuteron photoeffect extending into the energy region of this experiment (136 to 293 Mev) have been made by Marshall and Guth[6] and Schiff,[7] making various assumptions about the nuclear forces.

When the experiment reported herein was undertaken, experimental results at high energies had been published by Benedict and Woodward,[8] Kikuchi,[9] Littauer and Keck,[10] and Gilbert and Rosengren.[11] These experiments established some of the qualitative features of deuteron photodisintegration, but there were disagreements as to the angular distribution and magnitude of the total cross sections. In view of these inconsistencies in the existing data and because of the fundamental nature of the reaction, it was thought advisable to do the experiment at this laboratory using a different experimental technique.

Before this work was completed, results of high-energy experiments at California Institute of Technology, Cornell University, and University of Illinois were reported. A comparison of those results with results of this experiment is made in Section V-B.

II. EXPERIMENTAL METHOD

A. General Description

A diagram of the experimental arrangement is shown in Fig. 1. The photon beam was produced by the high-energy electron beam striking a 0.020-inch platinum target in the 335-Mev synchrotron. After suitable collimation the beam entered a liquid deuterium target. The events of interest are those in which the gamma ray disappears and a neutron and a proton emerge in roughly opposite directions. In this experiment only the proton was detected. Since this is a two-body reaction, measurement of the angle of emission of the proton and its energy is sufficient to determine the energy of the photon producing the event. The dynamics of the reaction are discussed in Section II-D and Appendix A. Care must be exercised to discriminate against protons produced by other reactions.

Protons were detected with a scintillation counter telescope consisting of a series of either twelve or thirteen counters with intervening copper absorbers. Coincident pulses from two of these counters triggered the sweep on an oscilloscope whenever a sufficiently heavily ionizing particle went through the first part of the telescope. Pulses from all but one of the counters were delayed, combined, and presented on the oscilloscope sweep. These sweeps were photographed individually and the required information was later read from the film. The height of the pulse from one of the counters near the beginning of the telescope determines the rate of energy loss of the particle, and the number of pulses from the subsequent counters determines, within limits, the range of the particle. These two pieces of information were generally sufficient to tell whether or not the particle was a proton. Once the particle is identified, the range measurement gives the energy of the

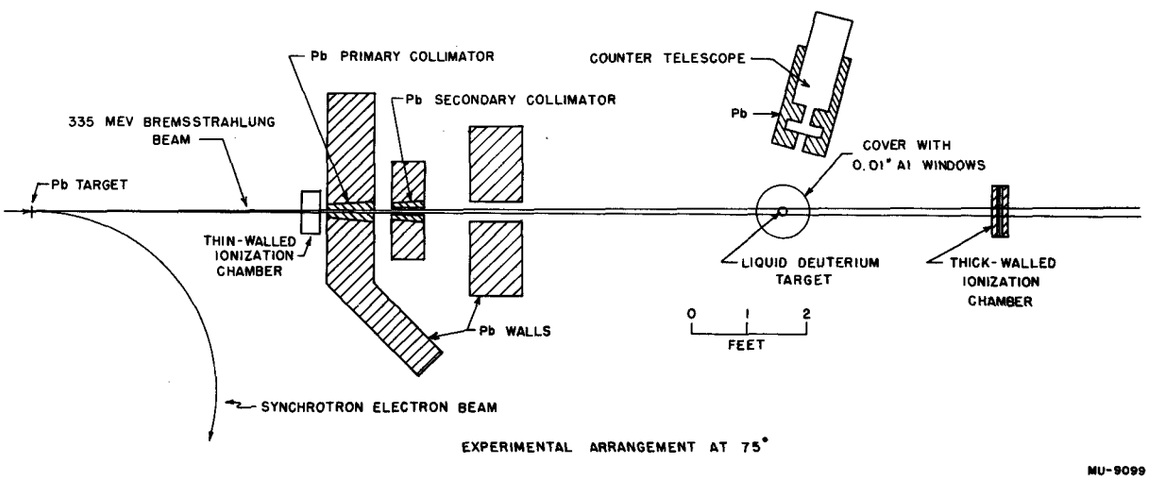

Fig. 1. Experimental Arrangement at 75°.

proton and this, together with the angle of emission as determined by the position of the counter telescope, gives the energy of the photon producing the disintegration.

It was desired to measure differential cross sections for photo-disintegration of deuterons by photons of various energies. These cross sections, when integrated, give the total cross section as a function of energy. Differential cross sections were measured at laboratory angles of 36°, 49°, 75°, 106°, and 141°. These correspond to center-of-mass angles of approximately 45°, 60°, 90°, 120°, and 150° for a photon energy of 240 Mev. Measurements were made at nine energies ranging from 136 Mev to 293 Mev. At 36°, however, no cross section was measured at 136 Mev because of interference by protons from events where mesons are produced. At 141° no cross sections were obtained at the two lowest energies because of the low-energy cutoff of the proton counter telescope.

Data to be reported here were taken during two synchrotron runs. In the first run cross sections were obtained at 49°, 75°, 106°, and 141°. Cross sections at 49° and 36° were measured in the second run. In the sections that follow, the experimental arrangement for the first run is described. The modifications in the equipment for the second run are described in Section II-G.

B. Photon Source

The maximum electron energy in the synchrotron at the target radius with a peak magnetic field of 11,400 gauss was taken to be 335 Mev. This is based on pair spectrometer measurements made by Anderson, Kenney, and McDonald.[12] They report, however, that a later and more precise value is 342 ± 6 Mev. The difference between this value and 335 Mev, which was used in the calculations, is negligible compared to other uncertainties in the experiment.

To reduce accidental counts, the machine was operated with a beam-pulse duration of about 3500 μsec. This is accomplished by gradually reducing the rf accelerating voltage near the end of the accelerating part of the cycle so that the electrons spiral in and strike the internal 0.020-inch platinum target from about 1750 μsec before the peak magnetic field is reached until about 1750 μsec after. Madey[13] discusses this process and gives references relating to it.

The basic photon energy spectrum used was that calculated by R. Christian following the Bethe-Heitler bremsstrahlung theory using a Thomas-Fermi model of the atom. This spectrum is modified by the finite target thickness as a result of energy loss by the electrons in the target and absorption of photons in the target. Powell et al.[14] give the spectrum as calculated by Christian for an infinitely thin target, and also that for a 0.020-inch platinum target. The spectrum must be further modified because of the spread in the energy of the electrons as they strike the target. During a beam pulse the magnetic field in the synchrotron varies between about 10,650 gauss and the peak value of 11,400 gauss. Since the magnet current is a sinusoidal function of time, the energy of the electrons as they strike the target can be expressed as $E = 335 \sin\left[(7790 - t)/7790\right] 90^{\circ}$, where t is the time in microseconds before peak field, 335 is the peak electron energy in Mev, and 7790 is the time in microseconds for one-quarter cycle of the magnet current. The beam intensity as a function of time was determined by photographing an oscilloscope presentation of the output of a scintillation counter placed in the beam. A marker was superimposed to indicate the position of peak magnetic field, and time markers established the time scale. It was assumed that the rate at which electrons struck the target was proportional to the output of the scintillation counter. Bremsstrahlung spectra corresponding to electron energies at various times before and after peak field were

drawn, weighted according to the output of the scintillation counter at the time and combined to give the final spectrum. Figure 2 shows (a) the thin-target spectrum computed from the Bethe-Heitler formula, (b) the spectrum corrected for the thick target, and (c) the spectrum with the additional correction for the electron energy distribution.

The angular distribution of photons of energy 300, 235, and 170 Mev in the bremsstrahlung beam has been measured by Anderson, Kenney, and McDonald.[26] Their data are given in Fig. 3. The relative beam intensity for an electron energy of 342 Mev and for various photon energies is plotted as a function of the angle θ, measured with respect to the beam axis. The curve is a function given by Lanzl and Hansen[15] with parameter $bT = 244\ m^2c^4$.

At 56 inches from the synchrotron target the beam was collimated by a tapered hole in a nine-inch lead block. The entrance end of the hole was 0.5 inch in diameter. The primary collimator was followed by a secondary lead collimator six inches thick with a hole just slightly larger than the beam. Another lead block six inches thick with a two-inch-diameter hole was placed between the secondary collimator and the deuterium target.

The beam was monitored with a thin-walled ionization chamber preceding the collimators and, during part of the experiment, with a Cornell-type thick-walled ionization chamber following the deuterium target. The measurement of the total beam energy is discussed in Section IV-D.

C. Target

A liquid deuterium target designed by Mr. Roscoe Byrnes was used. Figure 4 is a drawing of the target. The system consists essentially of a heat-exchange condenser in which liquid hydrogen is allowed to evaporate through a coil which is in thermal contact with another coil

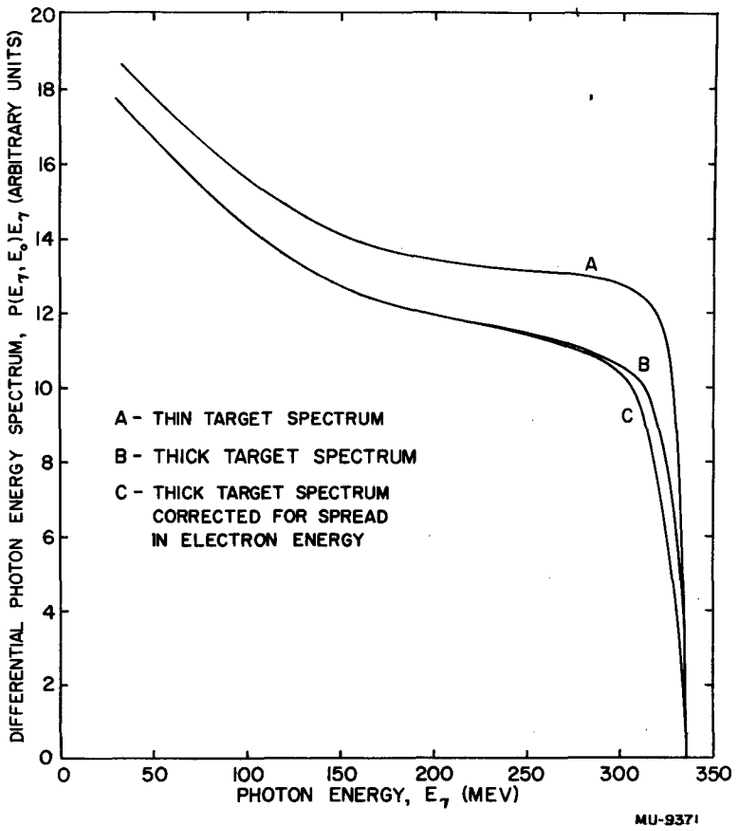

Fig. 2. Bremsstrahlung Spectra.

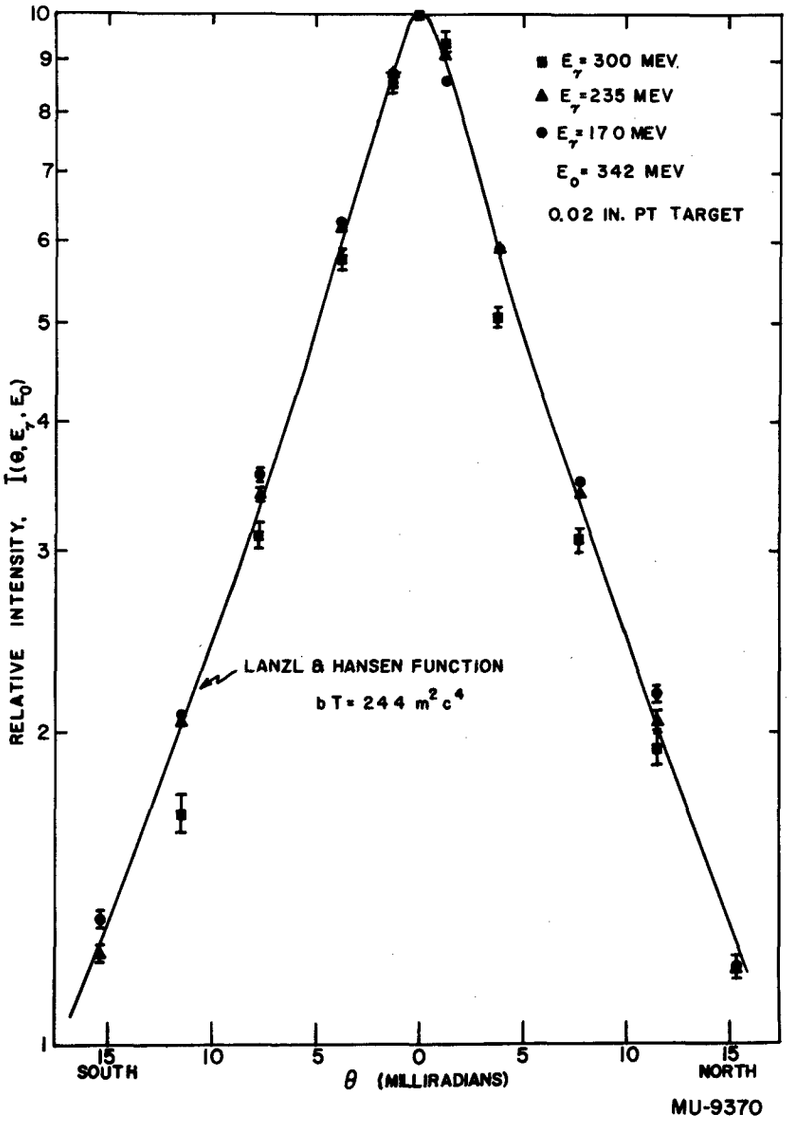

Fig. 3. Angular Distribution of the Bremsstrahlung Spectrum.

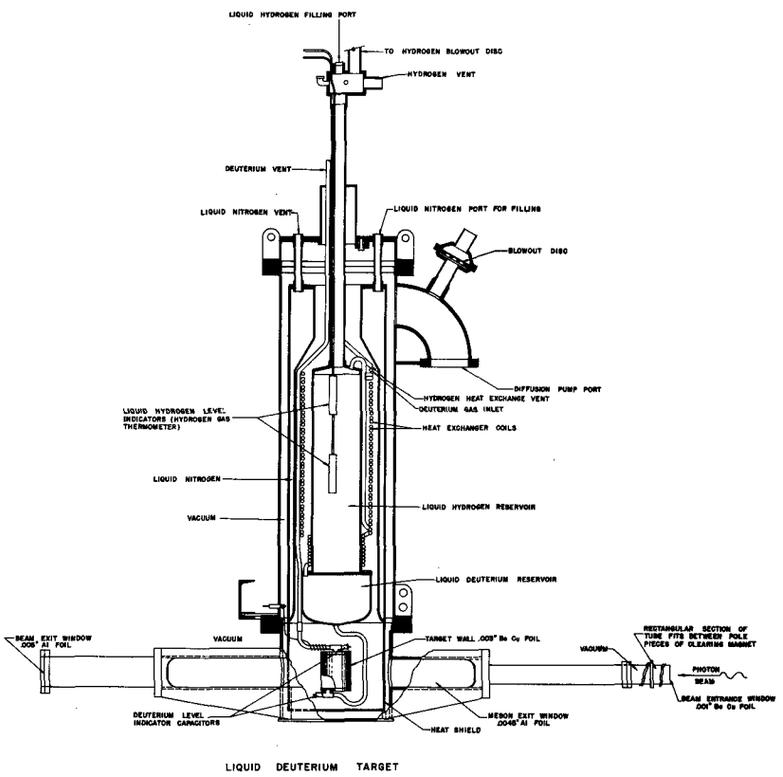

MUL-588

Fig. 4. Liquid Deuterium Target.

containing deuterium gas. Since the boiling point of deuterium at atmospheric pressure is almost 3.5° Kelvin higher than that of hydrogen, the deuterium condenses and collects in a liquid deuterium reservoir. A vertical cylinder, 1.5 inches in diameter with 2-mil brass side walls, was suspended below the reservoir and served as the actual target container. Provisions were made for emptying the target by closing one side of the deuterium target container. Evaporation from the surface of the liquid deuterium built up sufficient pressure to force the liquid deuterium out of the target into the reservoir. Small capacitors at the top and bottom of the target container served as sensing elements to determine whether the target was full or empty.

Analysis of the deuterium gas at the time of the runs indicated the presence of as much as 9 percent helium but negligible quantities of other gases. Since the helium does not condense at liquid-hydrogen temperature, it does not contaminate the liquid deuterium.

The vacuum chamber surrounding the target contained 10-mil aluminum windows through which passed the photon beam and the recoil protons. A heat shield at liquid nitrogen temperature surrounded the target. It contained holes for passage of the photon beam and consisted of 1-mil aluminum in the region where the protons emerged.

D. Proton Detector

The calculation of the dynamics of deuteron photodisintegration is outlined in Appendix A. Some of the results of this calculation are shown in Fig. 5, which gives proton kinetic energies as a function of laboratory angle for various photon energies. The upper and lower curves, labeled 306 Mev and 130 Mev, respectively, indicate the extreme photon energies that were of interest in this experiment. The vertical lines indicate laboratory angles at which cross sections were measured.

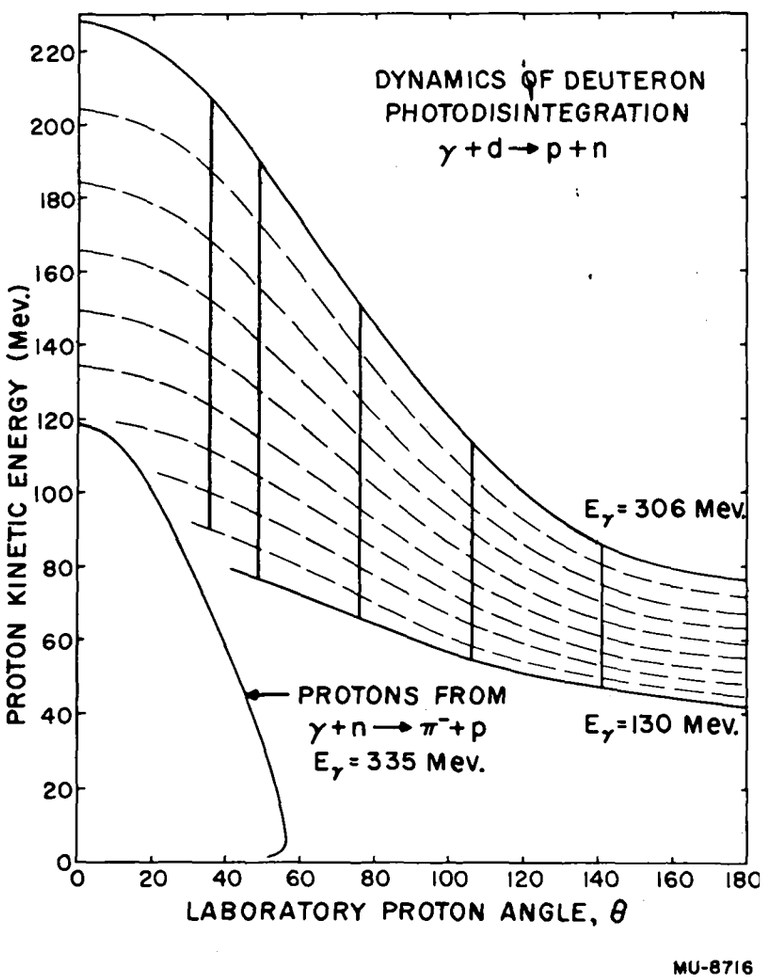

Fig. 5. Dynamics of Deuteron Photodisintegration.

It can be seen that the proton detector should be able to detect and measure the energy of protons in the interval of about 48 Mev to 205 Mev. The system must be capable of differentiating between protons and μ-or π-mesons. It must also be able to discriminate against electrons. The only known process of appreciable cross section whereby deuterons can be ejected from a deuterium target bombarded by photons is $\gamma + d \rightarrow \pi^{o} + d$. Deuterons from this process have a maximum energy of about 80 Mev for a photon energy of 335 Mev. The detector must be able to discriminate against deuterons up to this energy. In the system that was used, deuterons from the above process were not detected because of their limited range.

It was desired to select a proton detection system that was able to simultaneously detect protons of various energies, so as to reduce data-taking time.

The proton detector selected consisted of a scintillation counter telescope, which measured specific ionization and range of particles passing through it. The arrangement of counters and absorbers in the telescope is shown in Fig. 6. Counter C_2 consisted of a plastic scintillator 3 inches square and 0.5 inch thick. It was viewed by a 5819 photomultiplier through a tapered light pipe 7 inches long. The photomultiplier and scintillator were cemented to the light pipe with a commercial hard-setting transparent plastic. The height of the pulse from the 5819 is a measure of dE/dx, the energy loss of the particle in C_2. Counter C_2 was also viewed from one edge by a 1P21 photomultiplier. The output of this tube in coincidence with the output from a 1P21 viewing counter C_3 served to trigger the oscilloscope sweep upon which pulses from the counters were presented. C_3 consisted of a disk of plastic scintillator material 1.5 inches in diameter and 0.2 inch thick. It served to define the aperture of the counter telescope. C_3 was followed by a series of ten range counters

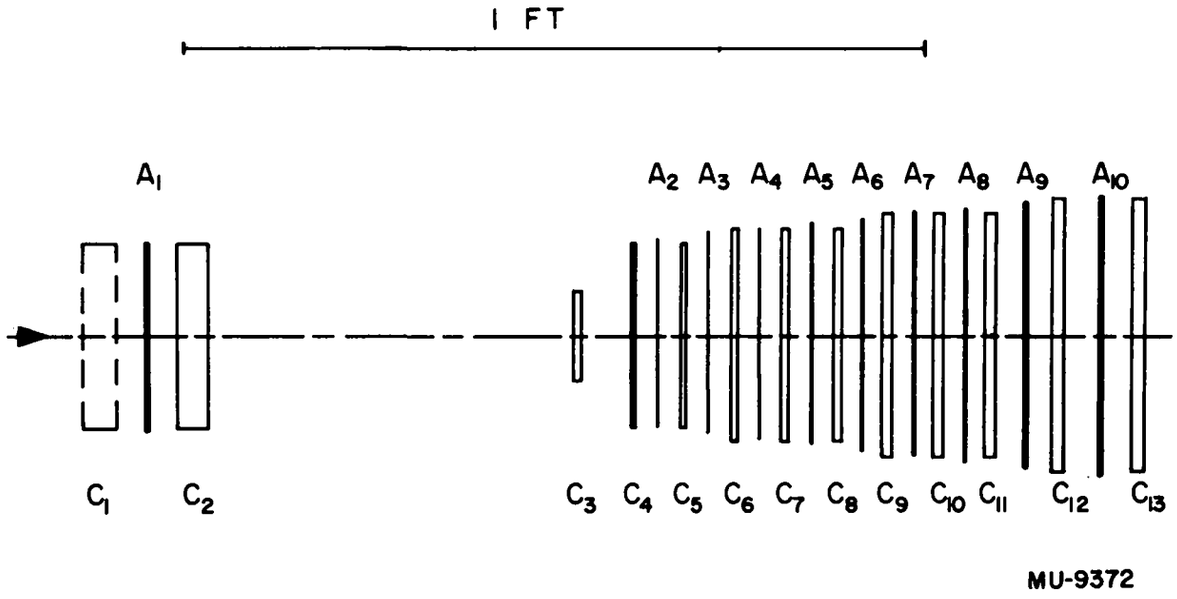

Fig. 6. Counter Telescope.

C_4 to C_{13}. These counters, together with copper plates A_2 to A_{10}, constituted an absorber with a means of determining how far a particle progressed through it. Counters C_4 through C_{13} were all circular plastic scintillator disks varying in size from 0.069 inch thick by 3 inches in diameter for C_4 to 0.175 inch thick by 4.5 inches in diameter for C_{13}. The size and position of the counters were such that particles passing through C_3 would have negligible probability of leaving the sides of the telescope owing to small-angle scattering. Each of the range counters was viewed from the edge by a single 1P21 photomultiplier. The tubes were mounted on alternate sides of the scintillators to reduce the over-all length of the telescope. All photomultipliers were shielded with double iron magnetic shields. The counter telescope was surrounded almost completely with a 2-inch layer of lead. In addition, lead blocks 4 inches thick with 2.5-inch-diameter holes were placed immediately in front of the telescope and between counters C_2 and C_3.

The counter was mounted on a cart which rotated on a large table. At all times the axis of the counter passed within a small fraction of an inch of the center of the effective target volume.

The dE/dx counter, C_2, had to be made thick enough to provide specific-ionization measurements accurate within a few percent. Rossi[16] gives the information necessary to calculate the spread in energy loss of particles as they pass through a counter. Measurements on the resolution of the 0.5-inch counter used in this experiment gave a resolution curve width at half maximum of ± 3 percent for 55-Mev protons and ± 8 percent for 205-Mev protons. In these measurements the proton energy was determined by its range in the counter telescope and there is, therefore, an uncertainty in proton energy of about ± 5 percent. An error in reading pulse heights from the film is also included. It is estimated at ± 1.5% to ± 3%, the higher value being for the higher energies. (A rough measurement of a counter only

0.2 inch thick in position C_2 gave a resolution of about ± 10% for 60-Mev protons. With this counter, the system did not give satisfactory separation between protons and mesons.)

A different set of copper absorbers was provided for each angle at which data were taken. The photon spectrum was divided into nine adjoining intervals having the following energy limits: 130, 143, 157, 173, 190, 209, 230, 253, 278, and 306 Mev. Figure 5 shows a curve of proton energy versus laboratory angle for each of these photon energies. For a given laboratory angle one can obtain from these curves a series of nine proton energy intervals corresponding to the above photon energy intervals. These intervals were commonly referred to as "channels" and they were numbered from one to nine. A proton reaching the first range counter C_4 but failing to reach the second range counter C_5 was, for example, said to fall in Channel 1. Absorbers A_1 through A_{10} were of such thicknesses that, for a given laboratory angle, the range channels in the counter telescope corresponded to the photon energy intervals described above. Thus if a suitable set of absorbers is used for each angle of observation, protons that fall in a given channel are those produced by photons in the corresponding energy interval. This is, of course, true only if we ignore finite target thickness, scattering, and range straggling, matters which are considered in Section IV-D.

At 36° no cross section was measured for Channel 1 because it was expected that this channel would be contaminated with protons from events in which mesons were produced. Figure 5 shows the maximum proton energy as a function of angle for such events, assuming the nucleons in the deuteron to be at rest. Because of the internal momentum of the deuteron, protons can appear at higher energies and larger angles than indicated in the figure. To eliminate Channel 1 at the 36° position, the absorber A_1 was increased in thickness so that protons reaching

counter C_4, but failing to reach counter C_5, correspond to Channel 2, etc. At 141° no cross sections were measured at Channels 1 and 2 because of the low-energy cutoff of the counter telescope. A proton must have an energy of about 52 Mev or more to go from the center of the target to the first range counter. Channel 1 and Channel 2 protons at 141° have energies lower than 52 Mev. Therefore, at this angle Channel 3 protons were made to stop in Channel 1, etc. The rather high-energy cutoff indicated above is due mainly to the thick dE/dx counter C_2 that was required to get suitable resolution when measuring high-energy protons.

E. Electronics

A block diagram of the electronic system is shown in Fig. 7. The rectangles shown in the counter telescope represent the scintillators and their associated phototubes with their power supplies and divider chains.

The part of the system that provides the oscilloscope trigger is essentially as described by Madey.[17] Negative signals from the anodes of the 1P21s in counters C_2 and C_3 are clipped to a time length of 5×10^{-9} seconds and limited in amplitude to about 3 volts by the clipper and limiter circuit whose diagram is shown in Fig. 8. The signals are then fed into a crystal diode double-coincidence circuit as given in Fig. 9. The coincidence output is amplified by two Hewlett-Packard Model 460A distributed amplifiers and fed into the trigger input of a Tektronix Type 517 oscilloscope. The gate formed by the oscilloscope whenever its sweep is triggered is fed to a scaler, which thus counts the coincidence output pulses. The oscilloscope trigger amplifier gain control serves as a discriminator. The single pulses from counters C_2 and C_3 are counted by taking small signals from the coincidence circuit monitor output and feeding them through Hewlett-Packard Model 460B distributed amplifiers and linear amplifiers to scalers.

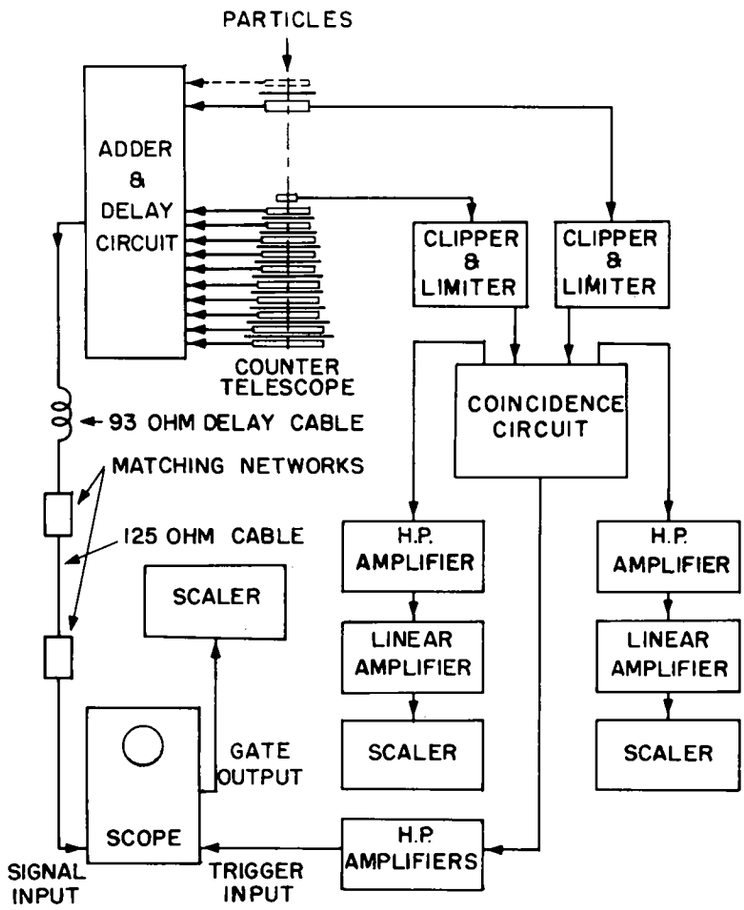

Fig. 7. Electronics Block Diagram.

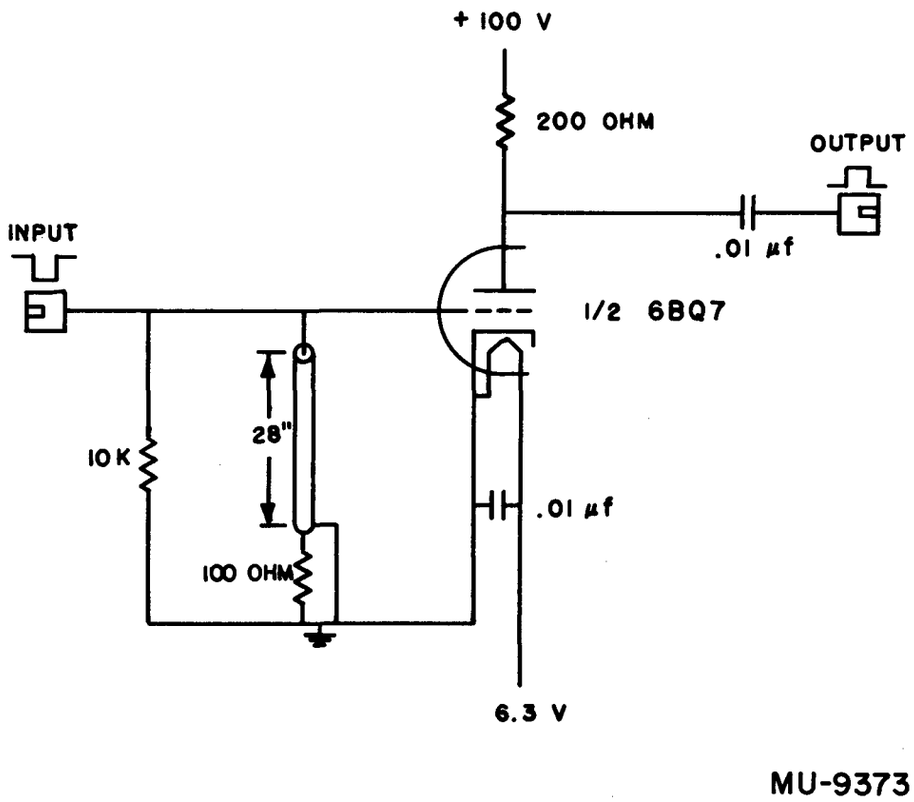

Fig. 8. Clipper and Limiter Circuit.

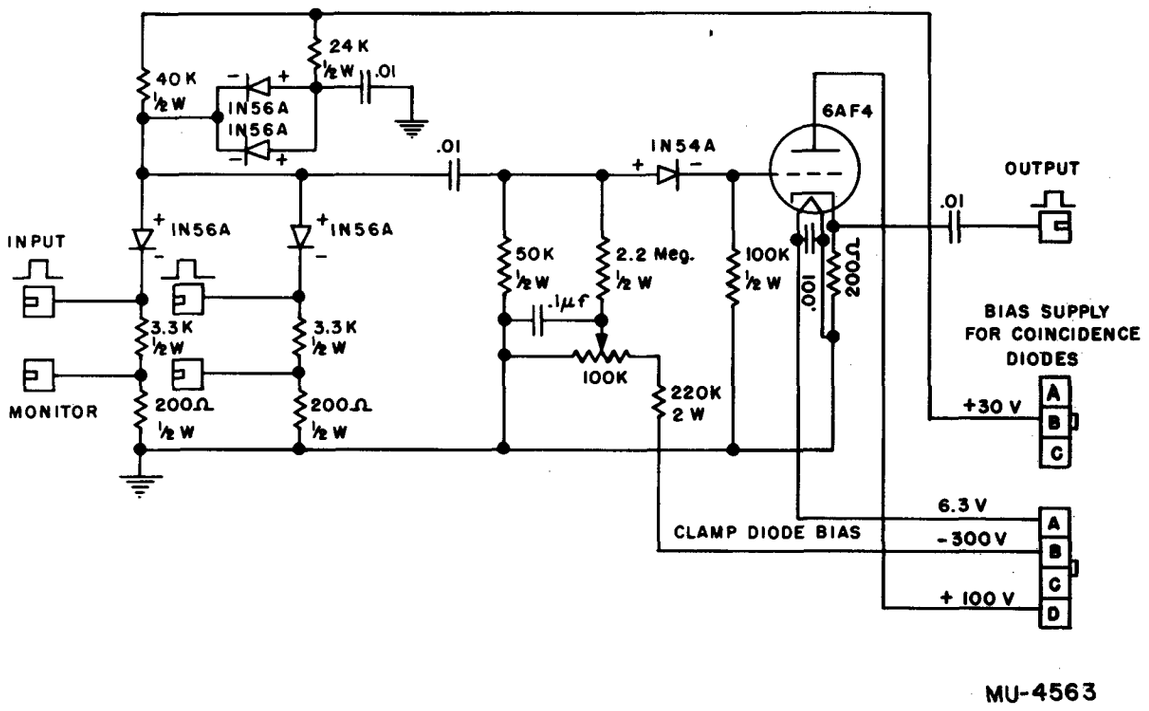

Fig. 9. Crystal Diode Double-Coincidence Circuit.

Signals from the 5819 phototube in counter C_2 and from the 1P21 phototubes in counters C_4 to C_{10} are combined in an adding and delaying circuit and connected through a length of 93-ohm delay cable, through the 125-ohm cable to the counting area, through two simple impedance-matching networks and an attenuator, to the signal input of the oscilloscope. Double-shielded 93-ohm delay cable was used in the synchrotron magnet room to reduce rf pickup. A few db of attenuation was used in the line to reduce reflections. The pulses are amplified by the distributed amplifiers in the oscilloscope and presented on a one-microsecond sweep. The adder and delay circuit is shown in Fig. 10. It consists of a long coaxial line with the phototube anodes connected to the center conductor at about 50-foot intervals. Matching coils of 0.04-μh inductance were used for connecting the anodes into the line. This value of inductance was calculated from the phototube anode capacity and the line impedance. It is not certain that these inductances are essential; their inductance is of the order of magnitude of the inductance of the anode lead in the tube. The line was terminated in a 93-ohm resistor at the end which was connected to Counter C_{10}. The 50-foot lengths of 93-ohm cable were stored on a spool mounted on the counter telescope chassis behind counter C_{10}.

A single high-voltage supply was used for range counters C_4 through C_{10}, but variable resistors were provided for adjusting individual phototube voltages. The voltages were adjusted to give approximately uniform pulse heights when 340-Mev protons traversed the counter telescope.

F. Photographic Method

A General Radio 35-mm oscilloscope camera was used to photograph the oscilloscope traces. Eastman Linagraph Pan film was moved continuously through the camera at rates such that about 30 traces per foot of film were recorded. With a sweep speed of 100 millimicroseconds

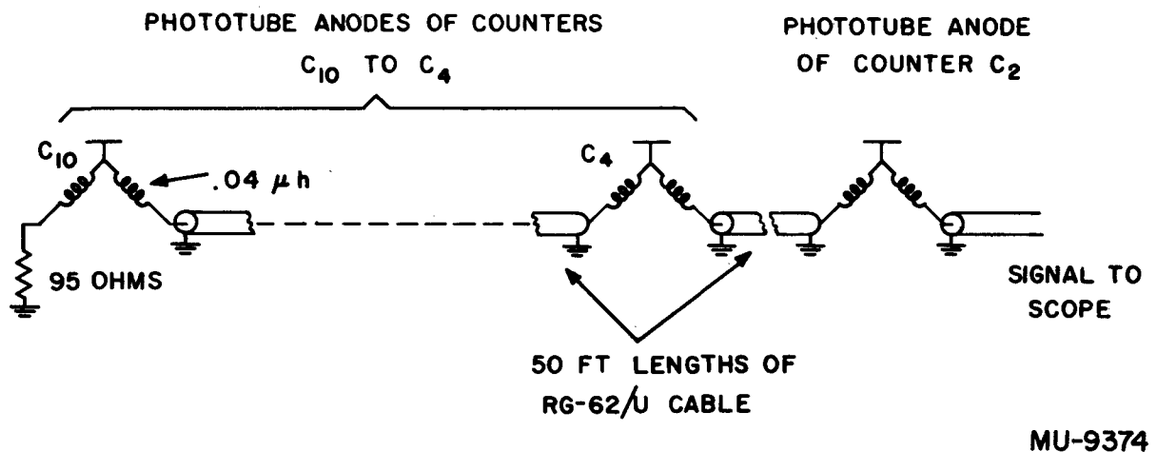

Fig. 10. Adder and Delay Circuit.

per cm and an aperture of f/2 it is possible to turn the oscilloscope intensity down below its maximum setting to give a very fine line. After development the number of pulses on each sweep and the height of the pulse from C_2 were read with the aid of a Recordak Film Reader and a suitable paper scale.

Examples of oscilloscope traces obtained with the above arrangement are shown in Fig. 11. These examples are discussed in the section on the treatment of data.

G. Apparatus for Second Synchrotron Run

After the first synchrotron run several changes were made in the apparatus to reduce background and improve particle identification. The general arrangement was similar to that shown in Fig. 1 with the following exceptions: To remove electrons from the incident photon beam a small sweeping magnet was placed between the second and third collimators. The plane of the magnet gap was vertical, so that electrons and positrons were swept out of the plane of the beam and telescope axis. The cover surrounding the deuterium target was provided with long pipes to remove the beam entrance and exit windows from the vicinity of the target proper. The pipe on the entrance side extended through the sweeping-magnet gap so that the entrance window preceded the sweeping magnet.

The deuterium container was changed from 1.5 inches in diameter to 4 inches in diameter. The thickness of the brass walls remained at 2 mils. With this target arrangement, the target-full : target-empty counting ratio was considerably increased. The hole in the lead block preceding the counter telescope was increased in width to 3 inches because of the wider proton source.

Experience gained in the first synchrotron run led to the belief that at forward angles spurious counts were occasionally obtained. It was

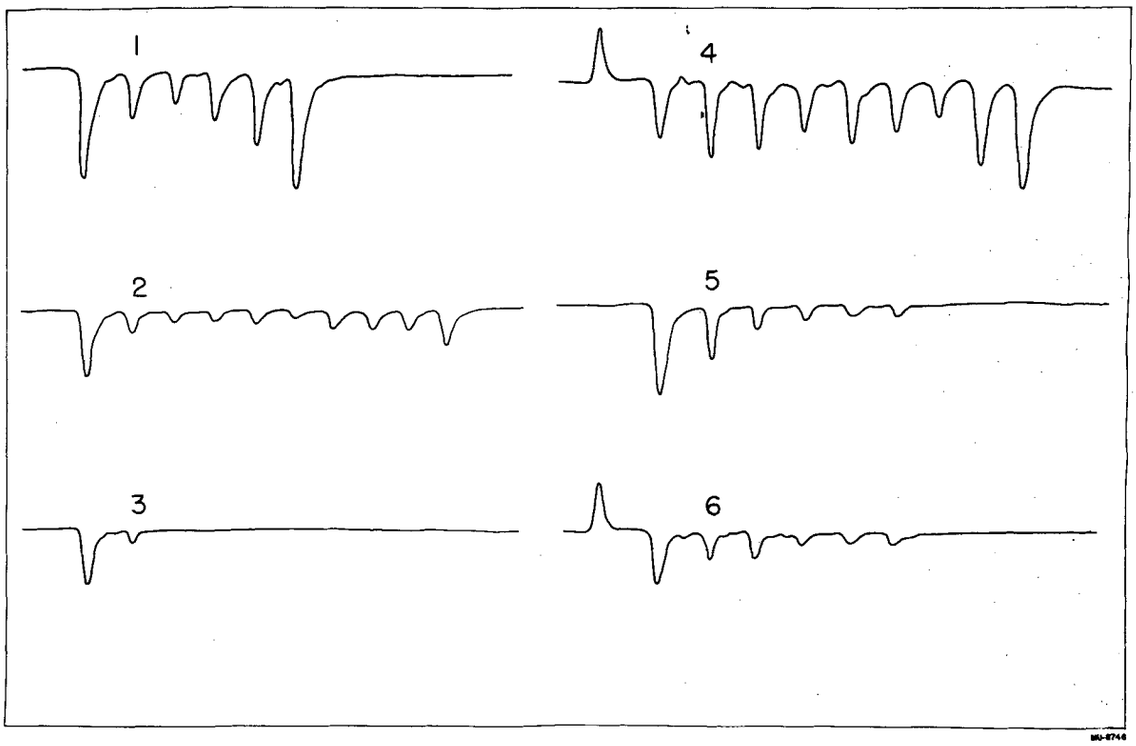

Fig. 11. Examples of Oscilloscope Traces.

suspected that a photon might convert in the thick Absorber A_1 and produce a group of electrons that could be mistaken for a proton. This problem is discussed more fully in Section IV-B. To discriminate against neutral particles, Counter C_1 was placed at the front of the counter telescope. It consisted of a plastic scintillator disk 3 inches in diameter and 0.535 inch thick, with a single 1P21 viewing its edge through a short light pipe. A signal from the last dynode of the phototube was fed to the adder and delay circuit. The pulse from this counter appeared at the beginning of the oscilloscope trace and with a polarity opposite from that of the other pulses.

In the first experimental arrangement the range counters had to be made quite thin because of the small proton energy intervals at 141°. When the telescope was used at forward angles where the proton energies are rather high, the signals obtained from the range counters were rather small. Also, one pulse would occasionally be missing from a series of range pulses. This suggested the possibility of insensitive spots in the thin plastic scintillators. A new set of scintillators was therefore constructed for use in the second run. The plastic from which they were made was tested for sensitivity with an ultraviolet light. The thicknesses of the counters were determined by the proton energy intervals at 49° and by the space available on the counter chassis. They varied in thickness from 0.356 inch for C_4 to 1.0 inch for C_{12}.

A Dumont Oscillograph Record Camera Type 321 was used in the second run. It was equipped with a device that closed the film-advancing solenoid for a fraction of a second each time a sweep was produced on the oscilloscope. The camera film speed was adjusted so that the film was advanced about 0.25 inch for each sweep.

III. COLLECTION OF DATA

The deuterium target was carefully aligned in the photon beam and the counter telescope cart was placed with its pivot directly under the center of the target. A scale on the large cart table provided an accurate means of measuring the laboratory angles. The alignment of the target in the beam was checked periodically with photographic plates. In the first run a 0.5-inch primary collimator was used. The beam diameter at the target was 1-3/8 inches, and the target diameter was 1.5 inches. Since the beam was almost as large in diameter as the target, it was necessary to maintain the target in accurate alignment. In photographs taken at the exit window of the target cover it was possible to see the deuterium container walls and their position relative to the beam.

Setting the operating level of the counting system presented no great problem. Since a photographic method is used to identify the protons, the principal requirement is that the counting device be at least sensitive enough to detect protons up to about 210 Mev. One does not want, however, to operate with excessively high sensitivity because of the high electron-counting rates encountered at forward angles. The oscilloscope trigger amplifier gain was set at such a level that 2-volt pulses 10 millimicroseconds long fed into the clipper-limiter circuits would just trigger the sweep. Then the voltages on the two coincidence phototubes were set at 1.6 kv. The tubes were selected to give approximately equal pulse heights when operated at equal voltages. Operation of the counter telescope in a low-intensity 340-Mev proton beam from the 184-inch cyclotron indicated that the lower end of the plateau for detecting protons of this energy occured at about 1.5 kv. During the first synchrotron run the counter was placed at 49° and operated with coincidence tube voltages ranging from 1.45 kv to 1.7 kv. Subsequent

analysis of the data indicated that 1.6 kv was a satisfactory operating point. In operation at 1.6 kv large numbers of mesons were always detected. Many of these particles produced smaller dE/dx pulses than the highest-energy protons. This was taken as evidence that the counter was detecting the protons with high efficiency.

During the run the counter was changed from angle to angle at frequent intervals. The target was frequently emptied for blank runs. It was found that placing a 2-inch lead brick in front of the counter telescope reduced the counting rate to essentially zero. This indicates that practically all counts were produced by particles coming through the lead channels from the direction of the target.

The total beam energy was measured using a Cornell-type thick-walled ionization chamber. Because of other experiments that were being done concurrently with this one, it was not always possible to have the Cornell chamber in place immediately behind the deuterium target. The thin-walled precollimator ionization chamber was used as a secondary standard, but it was calibrated in terms of the Cornell chamber at least twice per day. At no time did the ratio of the readings obtained from the two chambers vary more than ± 4% from the mean value, and generally the variation was somewhat less than this. Monitoring of the beam is considered in more detail in Section IV-D.

Attempts were made in both synchrotron runs to obtain cross sections at a laboratory angle of 24°. With the arrangement used, however, it did not prove possible to make a satisfactory separation of protons from the background. The difficulties encountered are discussed briefly in Section IV-B.

IV. TREATMENT OF DATA

A. Reading and Plotting of Data

The film was projected upon the screen of a Recordak Film Reader. The image size was approximately 4.5 times the size of the trace on the cathode-ray tube face. A special paper scale was constructed for use in measuring the height of the dE/dx pulse and the number of range pulses. The scale had a base line that was placed along the base of the image on the reader screen. The pulse-height scale had 2.2-mm divisions corresponding to 0.5-mm divisions on the cathode-ray tube face. The proton dE/dx pulses were generally 1 to 2 cm high on the cathode-ray tube or 20 to 40 divisions high on the scale. No attempt was made to read the pulse heights to less than one scale division. The reading error was estimated at ± 3% or less. Vertical numbered lines on the scale indicated the proper position of the range pulses relative to the dE/dx pulse. Unless a range pulse appeared within about 1/8 inch of its proper position along the base line it was not counted.

As the film was read, numbers giving the dE/dx pulse height and number of range pulses were recorded on a Soundscriber dictating machine. The data were later plotted from the records. In this manner something like 500 events per hour could be read and plotted.

Not every trace that appeared on the film was read. Events produced by electrons or low-energy mesons were easily recognized and were generally ignored. After reading a sample of a given group of data one could set a lower limit on the dE/dx pulse height to be read.

In reading the data from the second run there was the additional requirement that the positive pulse from counter C_1 be present. (See Trace No. 4 in Fig. 11). No particular use was made of the height of this pulse; only its presence in the proper position was required.

From the Soundscriber records a point for each event was plotted upon coordinate paper with the dE/dx pulse height as ordinate and number of range pulses as abscissa. Plots of two small samples of data are shown in Fig. 12.

B. Identification of Protons

In the data plots, one sees the proton points in a line fairly well separated from the mesons below. There are always some points in the region between the proton line and the mesons. Many of these points are due to protons that interact with nuclei in the range counters or the absorbers between them. A high-energy proton, for example, produces a relatively small dE/dx pulse and, if it happens to be absorbed or strongly deflected by a nucleus in the early part of the counter, it appears to stop in one of the early range channels. Thus a point somewhat below the proton line is produced. This effect is more serious at the forward angles. This is because of the wider range of proton energies involved at the forward angles and the resulting greater slope of the proton line.

In instances where there was any question as to where the line separating protons from mesons should be drawn, pieces of data taken under the same conditions were grouped together and histograms were drawn for the points in each range channel. Typical examples of such histograms are given in Fig. 13. In general, the separation improved upon going to lower energies and more backward angles. This is as expected because of the higher resolution of the dE/dx counter for lower-energy particles and because of the smaller slope of the proton line at backward angles.

Let us consider the sample traces in Fig. 11. Number 1 is found, upon being plotted with many other events from the same run, to be a proton. It entered the fifth range counter but failed to reach the sixth,

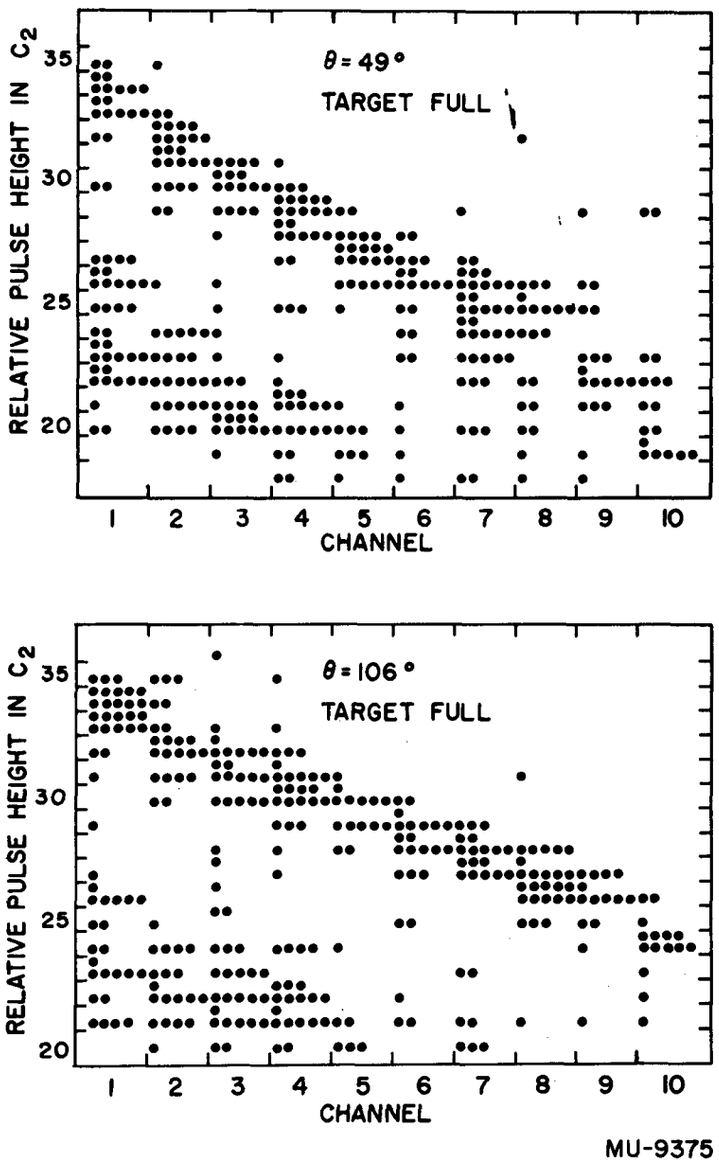

Fig. 12. Examples of Data Plots.

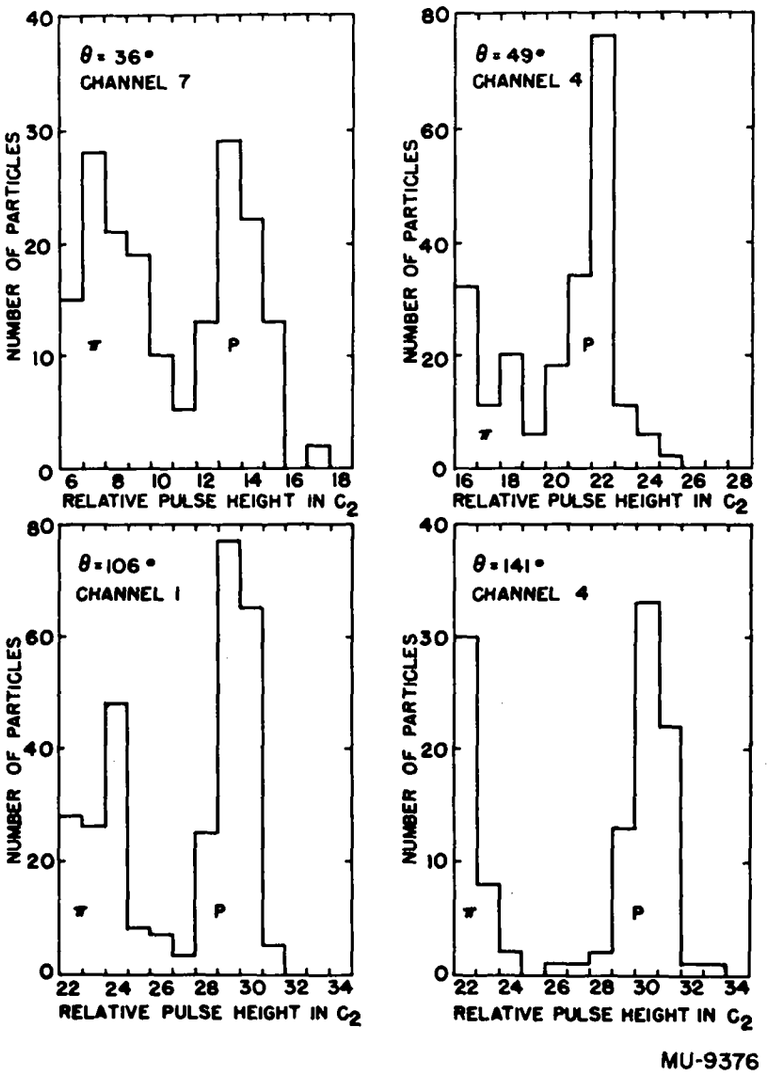

Fig. 13. Differential Pulse-Height Spectra in dE/dx Counter for Particles of Defined Residual Range.

it fell in Channel 5. Most events showed an increase in range pulse height as the particle slowed down. This was not always true, however, because the light collection was not very uniform in the range counters. Also, no great effort was made to adjust the voltage on the range counters to give the proper relative pulse height. Trace No. 2 was produced by a meson stopping in Channel 9. Trace No. 3 was probably produced by an electron. The counter telescope as it was used in this experiment did not make a clean separation between mesons and electrons. Traces 4 through 6 were taken from the second synchrotron run with counter C_1 in operation. Trace 4 represents a normal proton event. Since there is no positive pulse on Trace 5, it was apparently produced by an uncharged particle incident upon the counter telescope. The decreasing size of the range pulse causes one to suspect that the trace was not produced by a proton, but because of the nature of the range counters one does not feel justified in rejecting the event on this basis alone. Number 6 is an example of a troublesome type of event that occurred only very rarely at 49° but with increasing frequency at more forward angles. The formal requirements for a proton are fulfilled, but because of the small decreasing range pulse height one strongly suspects that it is not a proton. Events such as this were so numerous in the 24° data that a satisfactory proton separation was impossible.

C. Correction to the Proton Spectra

There is an appreciable probability that a proton in passing through the counter telescope will interact with a nucleus and be absorbed or strongly deflected. In other deuteron photodisintegration experiments where range or energy counters have been used, the correction for this effect has been calculated on the basis of assumptions about the cross sections and angular distributions involved. Yamagata et al.[18]

found that in the energy range of this experiment a maximum correction of 17.6% was obtained if the geometrical cross section was taken as the nuclear scattering cross section. On the assumption of total neutron cross sections, a maximum correction of 28.3% was calculated. This was taken as an upper limit to the correction. Gilbert and Rosengren[11] calculated a maximum correction of 40%, using geometric nuclear area. Because of the magnitude of the effect and the uncertainties in its calculation, the correction for the counter used in this experiment was determined experimentally.

The 340-Mev proton beam from the 184-inch cyclotron was used in making the measurements. Monoenergetic proton beams of various energies were generated by scattering the 340-Mev proton beam with a CH_2 target. Chamberlain et al.[19] and Hadley et al.[20] describe nucleon-nucleon scattering experiments and give formulas for the dynamics. Figure 14 gives the arrangement for the calibration experiment. Counter A detected one of the protons and Counters B and C detected the other. Signals from the three counters went to a triple-coincidence circuit, the output of which triggered the sweep of the Tektronix Model 517 oscilloscope. The counter telescope was placed immediately behind Counter A so that monoenergetic protons selected by the coincidence arrangement would pass through the telescope. Signals were fed from the counter telescope to the oscilloscope just as in the synchrotron runs except that the positive signal was taken from Counter A instead of the telescope Counter C_1.

To get proton beams with small energy spread it was necessary to use thin CH_2 targets and good angular resolution. Target thicknesses of either 0.59 g/cm^2 or 0.265 g/cm^2 were used. The incident proton beam was collimated with a 0.25-inch-diameter collimator. Counter A consisted of a plastic scintillator 3/8 inch wide by 1.5 inches high. Counters B and C were 3 inches high and had an effective width of 1 inch.

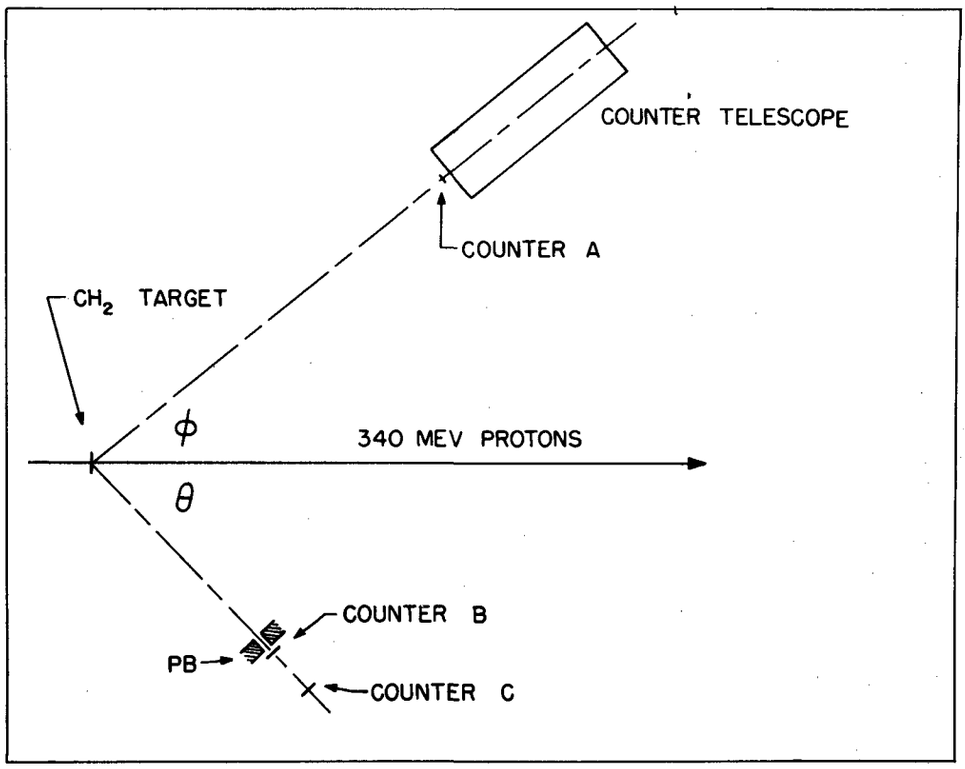

Fig. 14. Arrangement for Calibration Experiment.

With this arrangement it was possible to get proton beams of various energies with energy spreads comparable to or less than the channel width in the range counter. When a carbon target was substituted for the CH_2 target, the counting rate dropped to 20% or less of the CH_2 counting rate. Examination of the traces produced by these carbon events showed that in most cases the height of the dE/dx pulse was not correct for a proton of the energy under consideration. Thus the contribution from the carbon in the CH_2 target was negligible. With the angle ϕ set at a fixed value, the counting rate as a function of the angle θ was observed. Changing θ by $\pm$ 1.5° from its calculated value reduced the counting rate by about 60%, and changing θ by $\pm$ 2.5° reduced the counting rate more than 95%. Thus it appeared quite certain that only proton-proton scattering events were being observed.

To obtain information on the nuclear absorption for a given channel in the range counter and for a given set of range absorbers, the angle ϕ was set to give protons of the appropriate energy. Then θ was set at the angle calculated for the companion proton. About 1,000 counts were then taken and recorded photographically. Upon reading the film one could tell (a) how many of the protons failed to get to the range channel they should have reached, and (b) the apparent stopping point of those that fell short. The above process was repeated for each set of absorbers. In most cases three different proton energies were used for each set of absorbers.

Figure 15 shows the attenuation data obta ined. The percentages of protons lost before reaching various channels are plotted as functions of the set of absorbers in use. Figure 16 gives the same experimental points except that they are plotted versus range channel for various sets of absorbers. The curves drawn in the two figures are the result of an attempt to smooth the data in two directions. Percentages for use in the absorption correction were read from these curves.

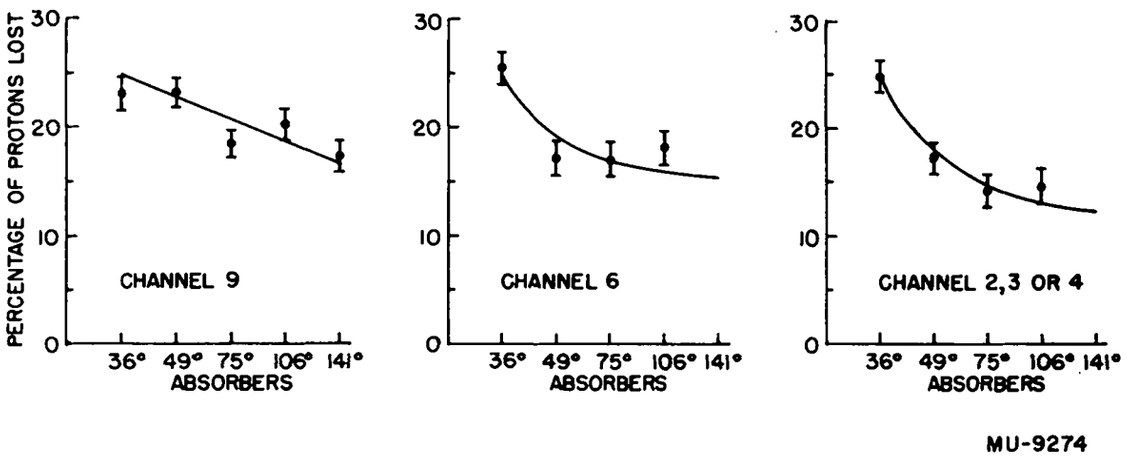

Fig. 15. Nuclear Attenuation as a Function of Angle.

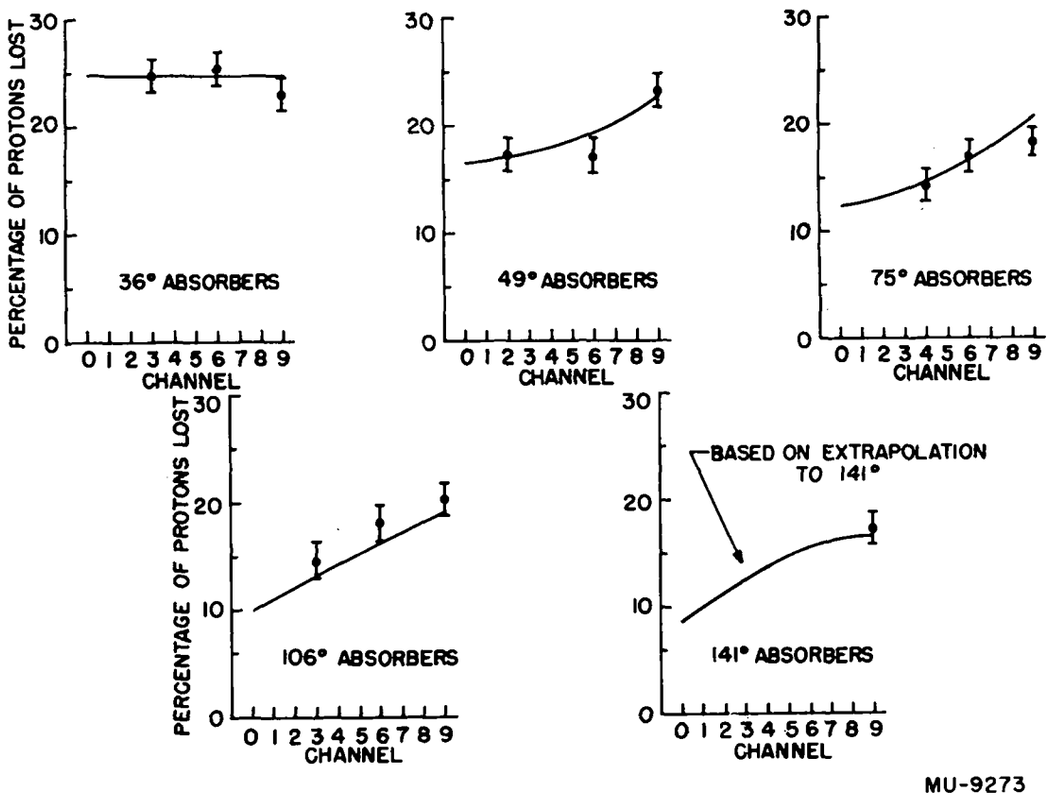

Fig. 16. Nuclear Attenuation as a Function of Range Channel.

When a proton interacted with a nucleus in such a way that it failed to reach the channel it should have, it was not lost completely but appeared to stop in some channel nearer the front of the telescope. Thus two corrections to the number of protons in a given channel were necessary. It was necessary to add a number to account for the loss of protons that should have reached the channel, and to subtract a number to account for protons that should have reached a higher channel but which appeared to stop in the channel under consideration. With the detailed data giving the fate of protons that failed to reach their proper channel, plots such as Fig. 17 were made for each set of absorbers. Consider, for example, the curve labeled Channel 7. It is concerned with incident protons of such an energy that they should have reached Channel 7. Percentages read from this curve give the percentage of these protons that appeared to stop in the channels preceding Channel 7.

In applying the nuclear absorption correction, actual plots of data such as those shown in Fig. 12 were used. Consideration was given to the position of the line separating protons from mesons. Some protons that fell short of their proper channel appeared to fall in the proton region, whereas others were below it. The maximum correction obtained was 26%.

D. Calculation of Cross Sections

The differential cross section for a given laboratory angle and a given photon energy is

$$\frac{d\sigma(\theta, E_\gamma)}{d\Omega} = \frac{(\text{protons in } \Delta Ep/\text{unit beam})}{\Delta\Omega(\text{photons in } \Delta E_\gamma/\text{unit beam})(\text{target deuterons/cm}^2)}.$$

Here ΔE_γ is one of the photon spectrum intervals described in Section II-D. E_γ is taken as the center of this interval. ΔE_p is the proton

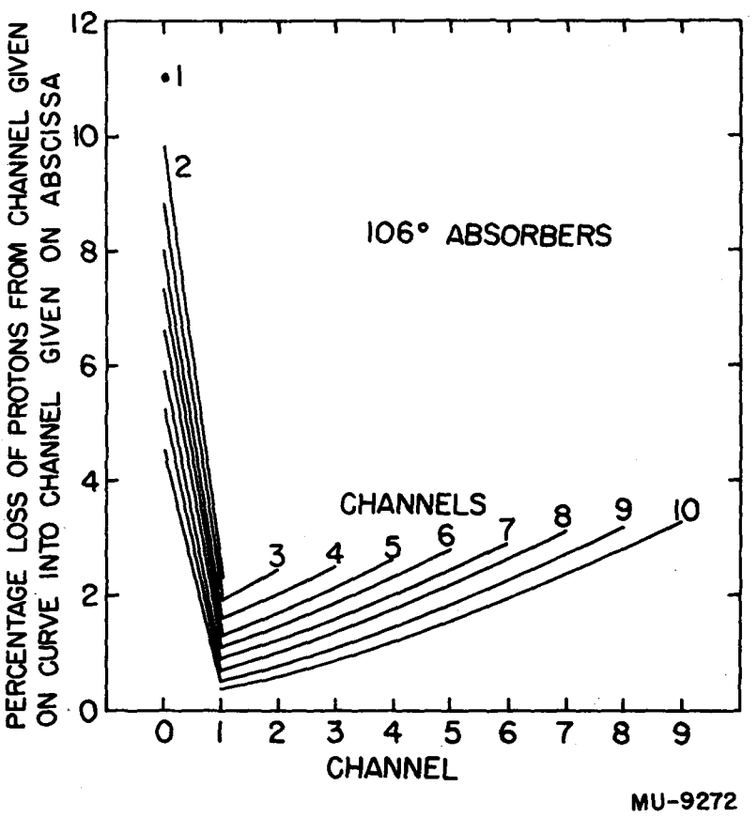

Fig. 17. Nuclear Absorption Corrections for 106° Absorbers.

energy interval corresponding to ΔE_γ. $\Delta\Omega$ is the proton detector solid angle.

Each of the quantities in the above expression is discussed and some consideration is given to the possible errors involved. The errors quoted for the differential cross sections are standard deviations due to counting statistics. The correction for absorption of protons in the counter telescope has been discussed in the previous section. A small additional correction due to absorption or scattering of protons by the deuterium in the target and the target walls might be called for, but the effect is small. It was estimated that the absorption in the target was comparable to that in Counter A in the experimental arrangement used in measuring the absorption correction. Therefore, no additional correction was made for target absorption. No correction was made for loss of protons due to multiple scattering. The counter was constructed with a small defining counter and large range counters to minimize this effect. The empirical correction obtained at the cyclotron should account in part, at least, for any multiple-scattering loss.

The number of protons in ΔE_p per unit beam to be used in the calculation of cross sections is obtained by subtracting the number per unit beam with the target empty from the number per unit beam with the target full. Typical target-full : target-empty ratios were 3.5 for the first synchrotron run and 7.0 for the second.

The principal sources of uncertainty in proton energy measurement are width of the range channels, variable energy loss in the target, and range straggling. If the width of a range channel represented the only uncertainty in determining the proton energy, we could specify the corresponding photon energies as being within about 4.8 % of the energy at the center of the photon energy interval. This is just the result of taking a photon energy interval width of 10% of the lower-limit energy.

The greatest uncertainty introduced by the target thickness is for the cross section measured at 141° and Channel 3. There the proton energy spread of ± 3.9 Mev corresponds to an uncertainty in photon energy of about ± 23%. This is a rather large uncertainty, but occurs in a region where the cross section changes very slowly with energy. A more typical value for uncertainty in photon energy because of target thickness is ± 2.3% for 75° Channel 5. In the second synchrotron run, with the 4-inch-diameter target, the above uncertainty ranged from ± 1.8% to ± 8.4%. The uncertainty due to range straggling is always a small fraction of the width of the range channels, and therefore is not very important. There may be a slight shift in the energy scale because a proton must penetrate a finite distance into a range counter before it can make a discernible pulse. It was found that 340-Mev protons expending 0.6 Mev in the thinnest range counter made a pulse several times the minimum discernible height. Therefore, even considering the lower light-producing efficiency of a proton coming to rest in a counter, it is thought that a proton of 1 Mev coming to rest in one of the range counters would produce a pulse of sufficient height. Thus the shift in energy scale due to the above effect is small and has been neglected.

The solid angle, $\Delta\Omega$, subtended by the proton counter is 3.35×10^{-3} steradian. Estimated errors in counter diameter, target-to-counter distance, and possible edge effects suggest a possible error of not more than 2% in the solid angle.

In the first synchrotron run the target diameter was 1.56 ± .008 inches at room temperature. The calculated shrinkage in cooling to liquid hydrogen temperature was 0.005 inch. The measured beam diameter at the target was 1.42 ± .01 inches. Because the beam was nearly as large in diameter as the target, and because of the non-uniformity of the beam intensity over the beam diameter, it was

necessary to calculate an effective target thickness. This thickness may be expressed by

$$\bar{x} = \frac{\int I_r \, \Delta x \, dA}{\int I_r \, dA}$$

where I_r is the beam intensity at radius r from the center of the beam, and Δx is the thickness of the target at the element of area dA. The integration is over the beam area at the target. I_r was obtained from the data of Anderson et al,[26] as given in Fig. 3. The above expression leads to a complete elliptic integral, which may be evaluated with the aid of tables. The resulting weighted target thickness is 1.348 inches. Woolley et al.[21] give 0.17041 g/cm^3 as the density of liquid deuterium at the normal boiling temperature of hydrogen. The effective number of target deuterons obtained from the above information should be in error by less than 1%.

In the second synchrotron run the target diameter was approximately 4 inches, while the beam diameter was approximately 5/8 inch. It did not prove necessary to calculate an effective target thickness as in the first experimental arrangement. The measured target thickness, adjusted very slightly for the variation in thickness over the beam area, was 3.95 ± 0.01 inch.

The unit of beam was taken as that required to produce 0.1 microcoulomb of charge in the precollimator ionization chamber. This chamber was frequently calibrated in terms of the Cornell-type thick-walled ionization chamber. The calibration of this latter chamber was taken as 3.74×10^{18} Mev total beam energy per coulomb of charge collected. This value is given for a chamber filled with air at normal temperature and pressure, and for an upper photon energy of 315 Mev. Correction was made for the actual pressure and temperature of the air in the chamber.

The above value for the Cornell-chamber calibration is subject to

some uncertainty. During the second synchrotron run the Cornell chamber was calibrated by use of the first method of Blocker et al.,[22] with a result of 3.34×10^{18} Mev/coulomb--a value about 11% lower than the 3.74×10^{18} Mev/coulomb calibration obtained at Cornell University.

A recent preprint from the California Institute of Technology[36] synchrotron group reported calibration of this type of chamber at 500 Mev. Using a pair spectrometer, they obtained a value of 4.75×10^{18} Mev/coulomb, and with a shower method, 4.12×10^{18} Mev/coulomb. They take the average value of 4.44×10^{18}, and state that it corresponds to 3.91×10^{18} at 300 Mev. If one then interpolates to get the value at 335 Mev, one obtains 4.00×10^{18}, which is 7% higher than the value used in this experiment.

The ratio between readings obtained in individual synchrotron runs with the precollimator chamber and with the Cornell chamber varied as much as ± 4% from the mean ratio. Sixty-three percent of the ratios were within ± 2%. For expressing the precollimator units of beam in terms of the Cornell units the mean ratio was used. It was felt that this was justified because the angle of observation and target were changed at frequent intervals during the experiment so that variations in the calibration of the precollimator chamber would tend to cancel out.

To obtain the number of photons in a given energy interval per unit of beam we consider the following expression for the total energy per unit of beam:

$$U = n\int_{o}^{E_o} P(E_\gamma, E_o)\, E_\gamma\, dE_\gamma.$$

Here $P(E_\gamma, E_o)$ is the relative probability for production of a photon of energy E_γ when the synchrotron target is bombarded with electrons of energy E_o. It is this quantity, corrected for spread in electron

energy and multiplied by E_γ, that is plotted as curve C in Fig. 2. Further, n is a number such that $nP(E_\gamma, E_o)$ gives the number of photons of energy E_γ per Mev in a unit of beam. The value of n was obtained from the above formula, by use of a numerical evaluation of the integral and the value of U as measured by beam monitor. The number of photons in an energy interval ΔE_γ is then

$$n\, P(E_\gamma, E_o)\, E_\gamma \Delta E_\gamma / E_\gamma .$$

V. RESULTS AND DISCUSSION

A. Differential and Total Cross Sections

Laboratory and center-of-mass differential cross sections for various energies and angles are given in Table I. The center-of-mass cross sections for various laboratory angles are plotted as a function of energy in Figs. 18 to 22. Figure 19 gives cross sections obtained in the first and second synchrotron runs. The agreement is seen to be satisfactory. For obtaining angular distributions and total cross sections, data from Channels 1 and 2, from 3 and 4, from 5 and 6, and from 7 and 8 were combined. The 49° data from the two runs were combined. Figures 23 to 27 show the angular distributions for laboratory photon energies of 143, 173, 209, 253, and 293 Mev. The curves shown in these figures are the result of fitting curves of the form $d\sigma/d\Omega' = A + B \cos\theta' + C \cos^2\theta'$ to the experimental points. Some notes on curve fitting are given in Appendix B. The ratios of the constants B and C to the constant A are plotted as a function of photon energy in Fig. 28. Integration of the angular distribution curves gives for the total cross section $\sigma_\tau = 4\pi(A + \frac{C}{3})$. Figure 29 shows the total cross sections as functions of energy.

B. Comparison with other Experiments

High-energy photodisintegration of deuterons has been under investigation at most laboratories where accelerators are available, and at least preliminary results on several of these experiments have been reported. For example, Keck et al.,[23] working at Cornell, measured angular distributions at photon energies of 180 and 260 Mev. They employed a counter telescope, which measured dE/dx and range. Their differential cross sections are shown with results of this experiment in Figs. 24 and 26. The total cross sections are included

Table I

Differential cross sections for photodisintegration of deuterons at various energies and angles. (θ = lab.; θ' = c.m.).

θ (Deg)	$\langle E_\gamma \rangle$ (Mev)	θ' (Deg)	Photons in ΔE_γ per unit beam	$d\sigma/d\Omega$ (μb)	$d\sigma/d\Omega'$ (μb)
36	150	42.8	0.503×10^8	12.7±0.9	9.6±0.7
	165	43.2	0.490	8.8±0.9	6.6±0.7
	182	43.5	0.482	8.5±1.1	6.3±0.8
	200	43.9	0.471	6.9±1.0	5.1±0.8
	220	44.4	0.462	9.9±1.0	7.1±0.7
	242	44.8	0.454	8.6±0.9	6.1±0.6
	266	45.3	0.443	10.5±1.0	7.4±0.7
	293	45.7	0.417	8.5±0.9	5.9±0.6
49 (Run II)	136	57.3	0.518×10^8	9.7±1.2	7.8±0.9
	150	57.7	0.503	10.1±1.4	8.1±1.1
	165	58.2	0.490	8.4±1.1	6.7±0.9
	182	58.6	0.482	7.9±1.2	6.2±0.9
	200	59.1	0.471	6.6±1.2	5.2±0.9
	220	59.7	0.462	8.3±1.0	6.4±0.8
	242	60.2	0.454	8.7±1.0	6.7±0.8
	266	60.8	0.443	8.0±1.2	6.1±0.9
	293	61.4	0.417	7.5±1.2	5.8±0.9
49 (Run I)	136	57.3	2.41×10^8	10.0±1.0	8.1±0.8
	150	57.7	2.34	7.3±1.0	5.8±0.8
	165	58.2	2.28	8.0±0.9	6.4±0.7
	182	58.6	2.24	8.9±0.9	7.0±0.7
	200	59.1	2.19	6.5±0.8	5.1±0.6
	220	59.7	2.15	7.8±0.9	6.1±0.7
	242	60.2	2.11	8.1±0.8	6.3±0.6
	266	60.8	2.06	8.9±0.9	6.8±0.7
	293	61.4	1.94	9.2±0.9	7.0±0.7

Table I (continued)

Differential cross sections for photodisintegration of deuterons at various energies and angles. (θ = lab.; θ' = c.m.).

θ (Deg)	$\langle E_\gamma \rangle$ (Mev)	θ' (Deg)	Photons in ΔE_γ per unit beam	$d\sigma/d\Omega$ (μb)	$d\sigma/d\Omega'$ (μb)
75	136	85.7	2.41×10^8	6.7±0.7	6.4±0.7
	150	86.2	2.34	8.0±0.7	7.7±0.6
	165	86.8	2.28	7.2±0.7	6.9±0.7
	182	87.3	2.24	6.2±0.7	6.0±0.7
	200	87.9	2.19	6.8±0.7	6.5±0.6
	220	88.6	2.15	6.2±0.7	6.1±0.7
	242	89.2	2.11	6.9±0.7	6.7±0.7
	266	89.9	2.06	7.5±0.7	7.3±0.7
	293	90.6	1.94	6.2±0.7	6.0±0.6
106	136	116.5	2.41×10^8	4.2±0.6	4.9±0.7
	150	117.0	2.34	3.7±0.5	4.4±0.6
	165	117.5	2.28	3.7±0.5	4.4±0.6
	182	118.1	2.24	3.3±0.5	4.0±0.6
	200	118.7	2.19	4.5±0.5	5.5±0.6
	220	119.3	2.15	4.7±0.5	5.9±0.6
	242	120.0	2.11	3.5±0.6	4.5±0.7
	266	120.7	2.06	4.8±0.5	6.1±0.6
	293	121.3	1.94	4.8±0.5	6.2±0.7
141	165	148.5	2.28×10^8	1.7±0.4	2.3±0.6
	182	148.8	2.24	1.8±0.5	2.5±0.7
	200	149.2	2.19	1.8±0.4	2.5±0.6
	220	149.6	2.15	2.6±0.5	3.8±0.7
	242	150.0	2.11	2.1±0.5	3.2±0.7
	266	150.4	2.06	3.1±0.5	4.8±0.7
	293	150.8	1.94	1.8±0.5	2.8±0.8

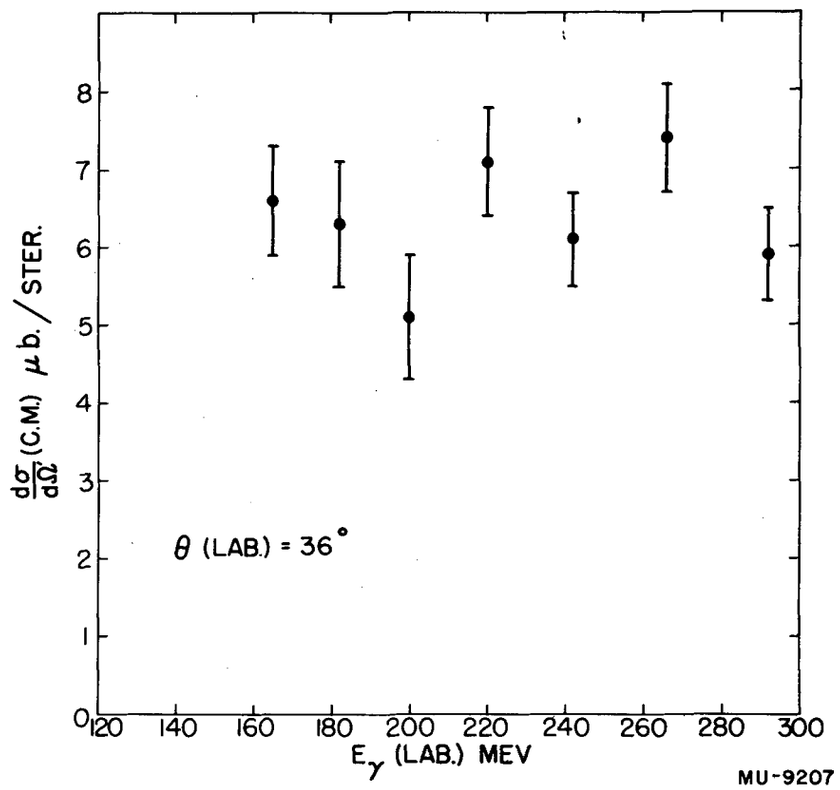

Fig. 18. Differential Cross Sections Versus Photon Energy for $\theta=36^{\circ}$.

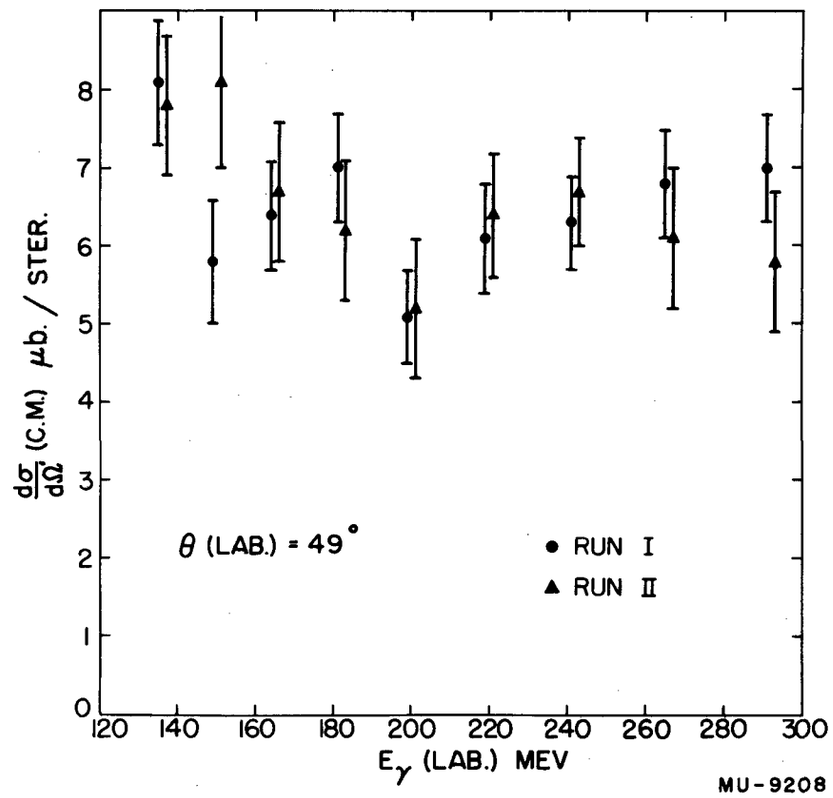

Fig. 19. Differential Cross Sections Versus Photon Energy for θ=49°.

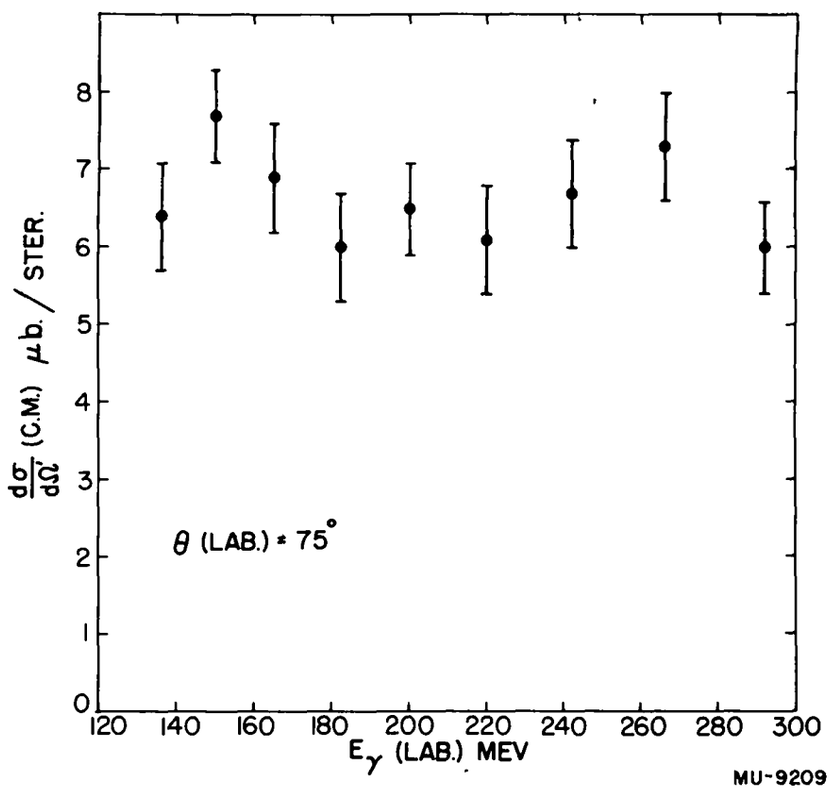

Fig. 20. Differential Cross Sections Versus Photon Energy for $\theta=75^{\circ}$.

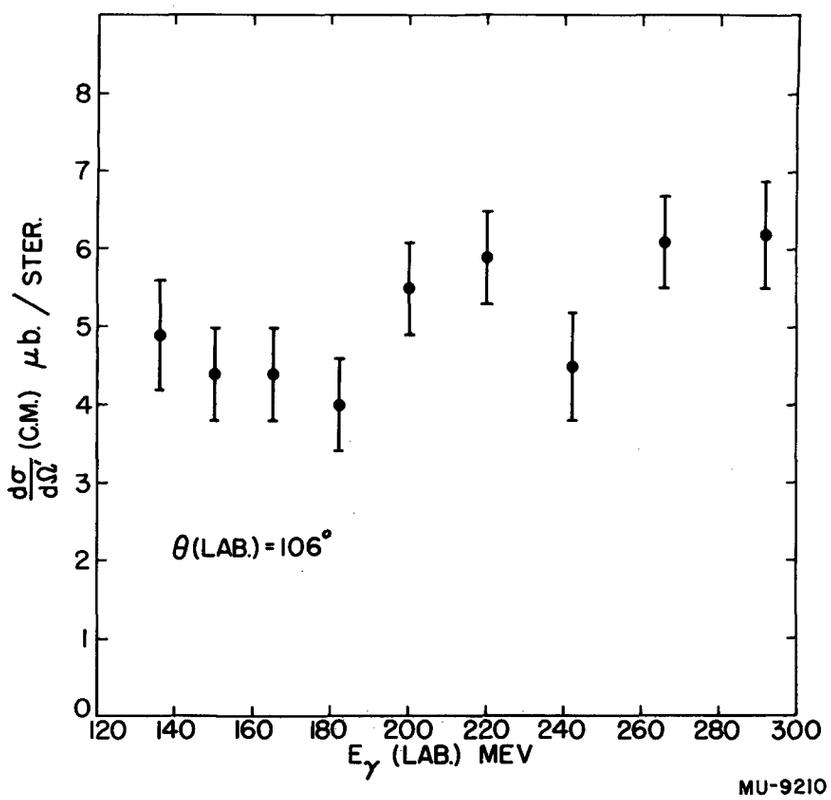

Fig. 21. Differential Cross Sections Versus Photon Energy for $\theta=106^{\circ}$.

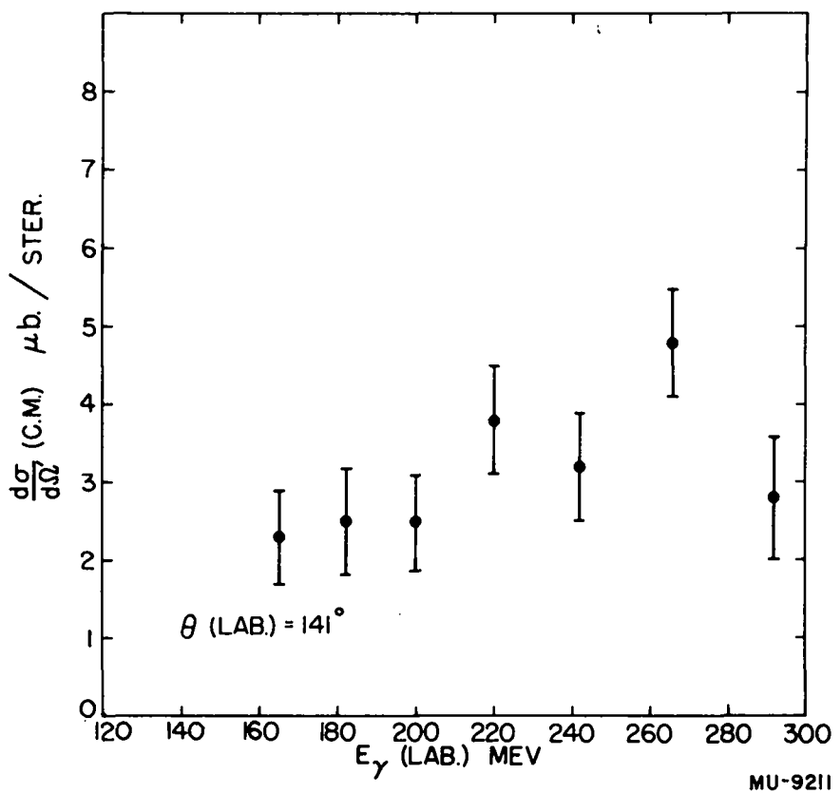

Fig. 22. Differential Cross Sections Versus Photon Energy for θ=141°.

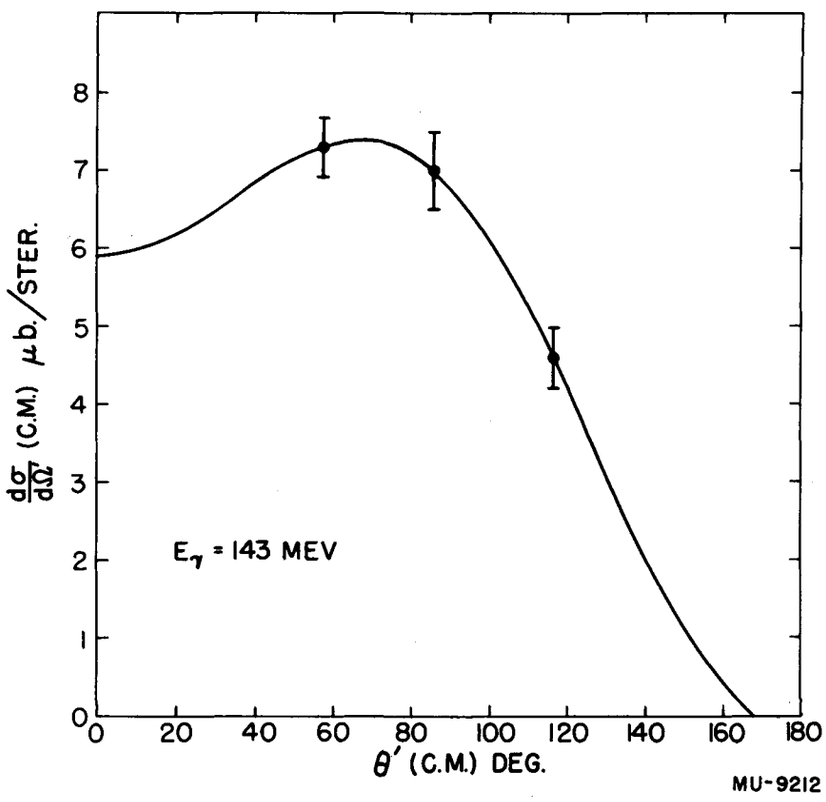

Fig. 23. Angular Distribution for E_γ = 143 Mev.

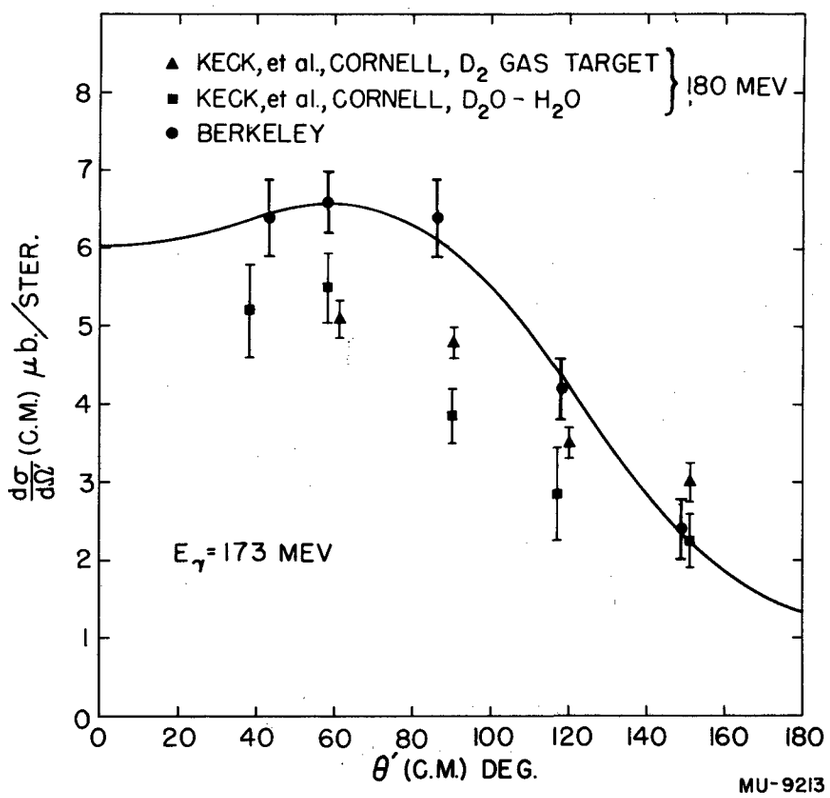

Fig. 24. Angular Distribution for E_γ = 173 Mev.

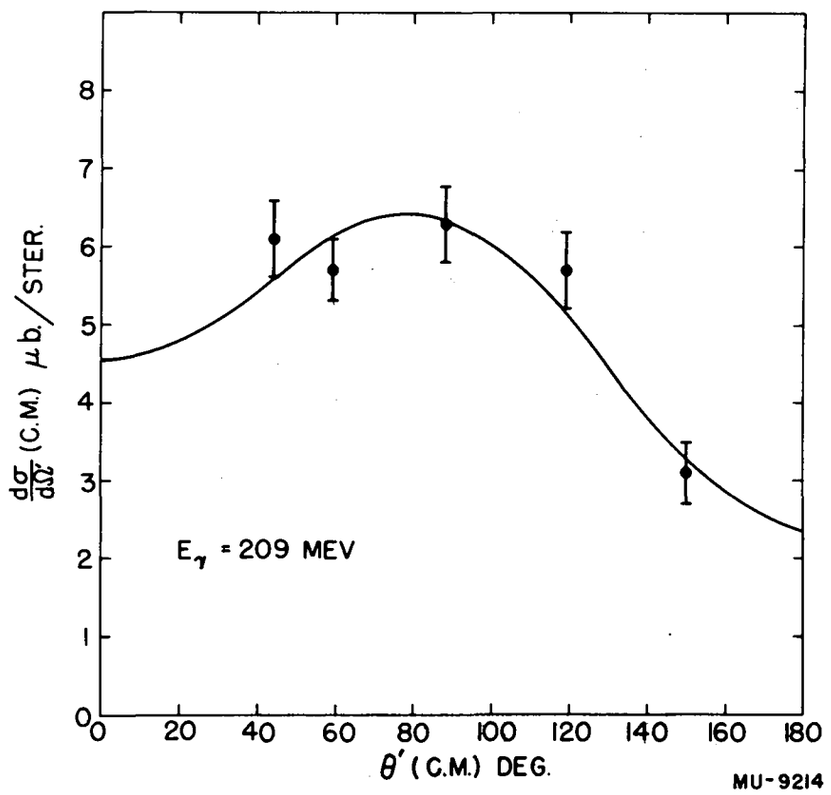

Fig. 25. Angular Distribution for E_γ = 209 Mev.

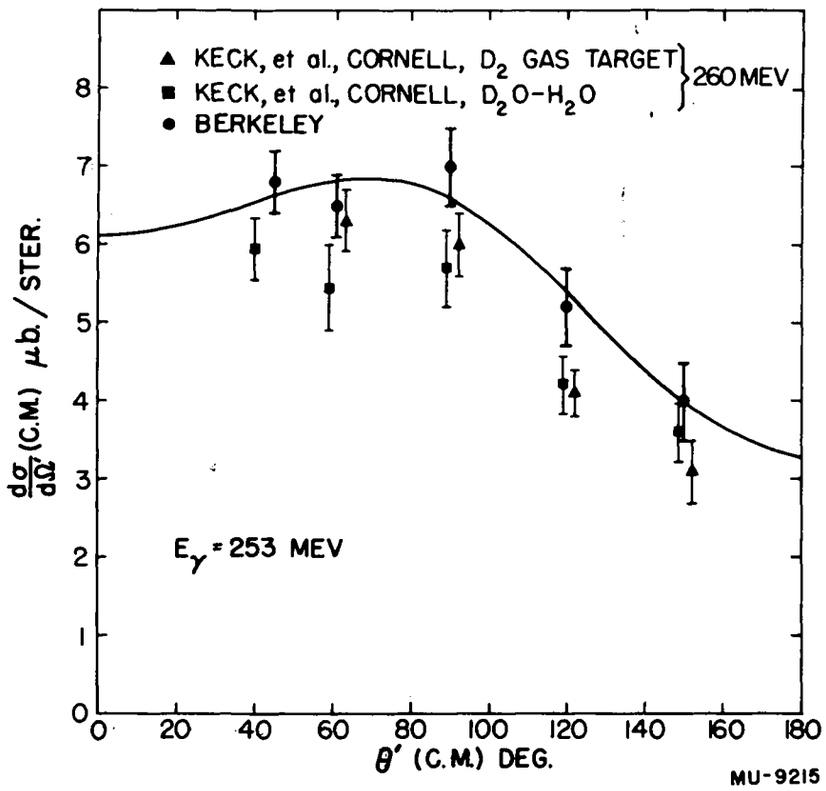

Fig. 26. Angular Distribution for E_γ = 253 Mev.

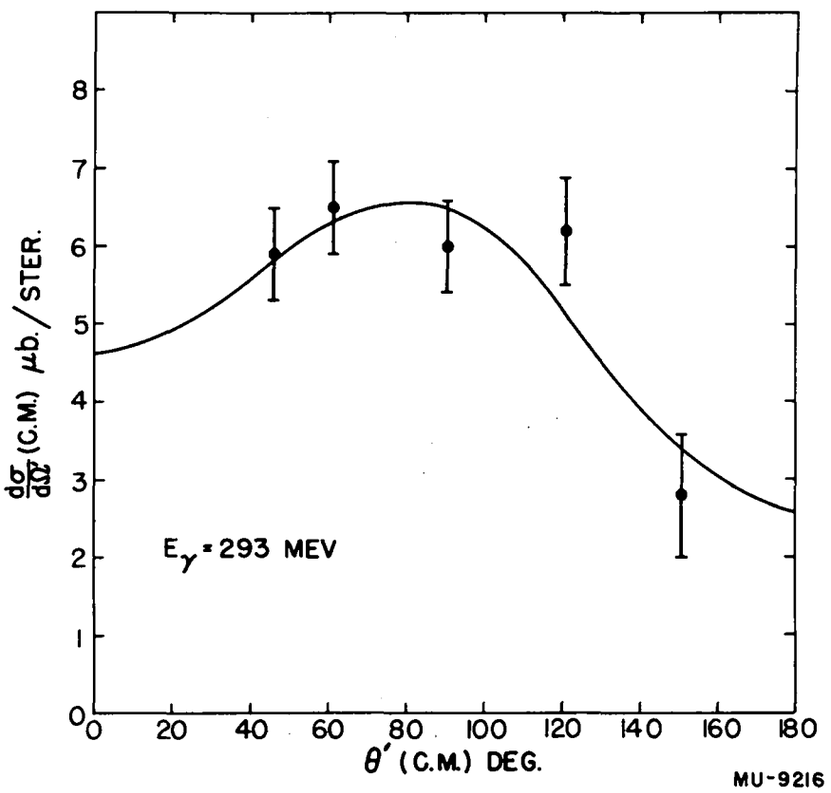

Fig. 27. Angular Distribution for E_γ = 293 Mev.

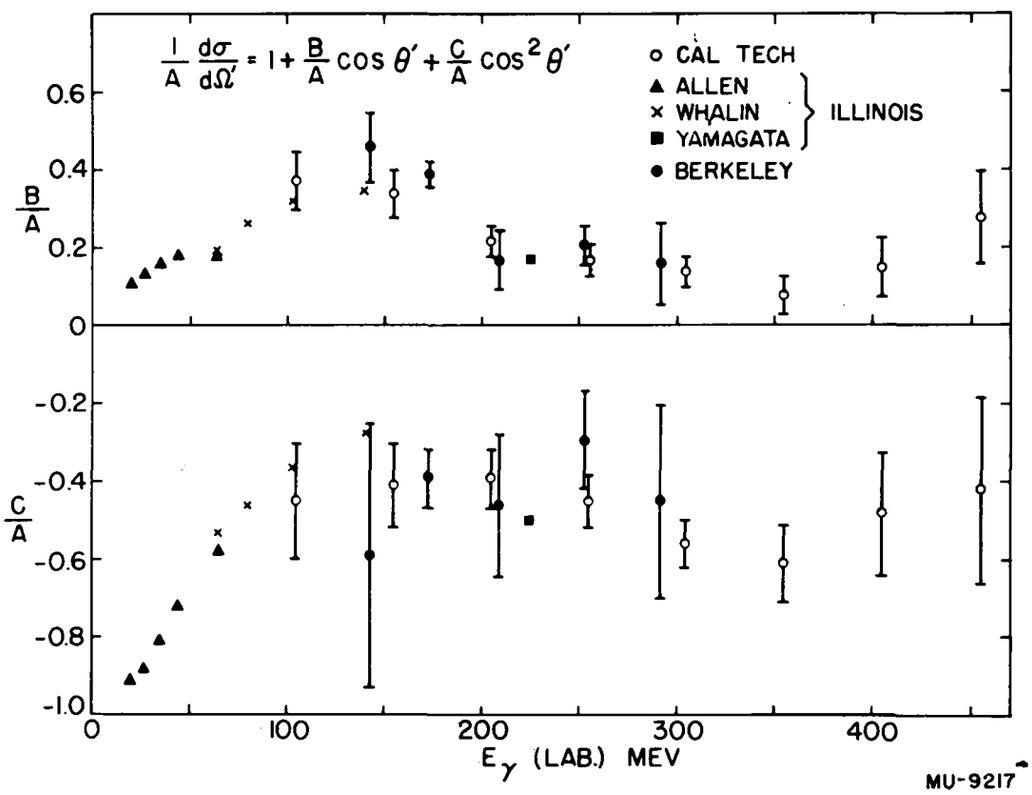

Fig. 28. Angular Distributions as Functions of Energy.

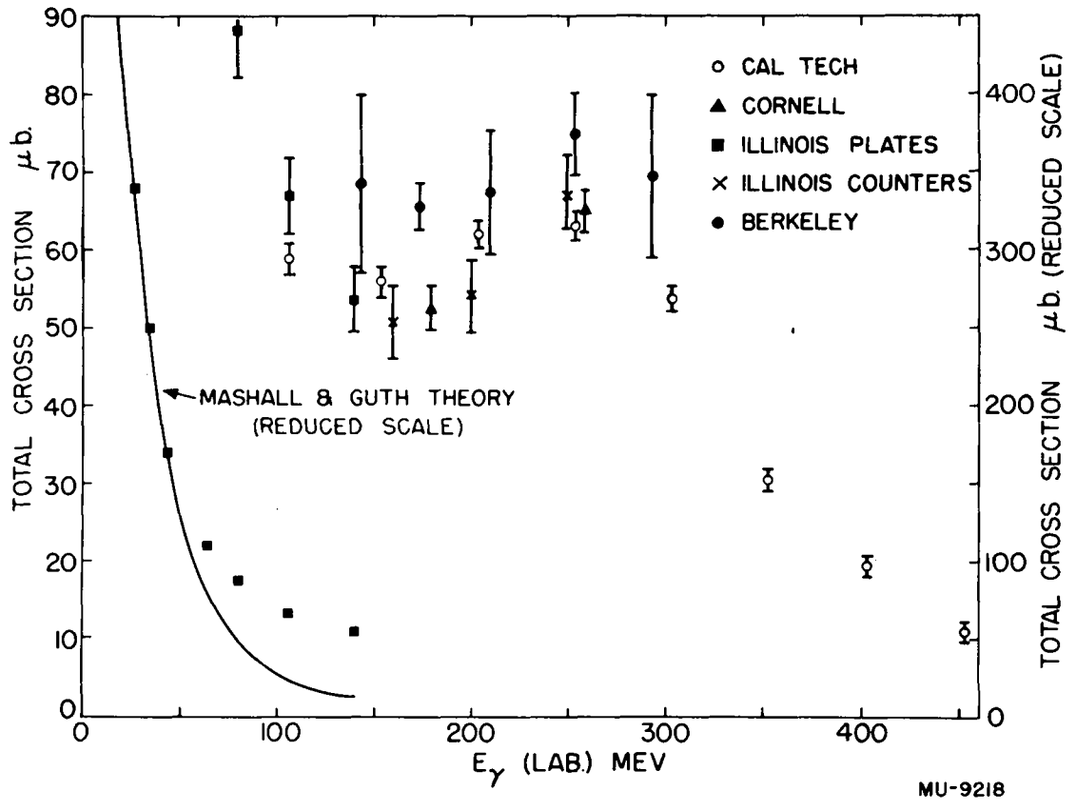

Fig. 29. Total Cross Sections as Functions of Energy.

in Fig. 29. A series of experiments at Illinois has covered the energy region from 20 to 260 Mev. Allen and Hanson[24] measured cross sections from 20 to 65 Mev using nuclear emulsions. An experiment extending into the energy region of this experiment was done by Whalin,[25] who also used nuclear emulsions. Yamagata et al.[18] used a proton counter telescope of five organic scintillators to measure cross sections at three angles and at energies from 142 to 260 Mev. Schriever et al.[27] used nuclear emulsions in an experiment extending from 70 to 235 Mev. Some of the results of the above experiments are compared with results of this experiment in Figs. 28 and 29. No errors are available for the ratios B/A and C/A in the Illinois experiments.

At California Institute of Technology, Tollestrup, Keck, and Smythe[28] have obtained excellent angular distributions at energies from 100 Mev to 450 Mev, using a counter telescope that measured dE/dx and range. The coefficients of the angular distributions and the total cross sections are given in Figs. 28 and 29.

It is seen from Fig. 28 that the angular distributions measured in this experiment are consistent with those obtained at other laboratories. In the energy region from 143 Mev to 293 Mev the $\cos\ \theta'$ term, representing the fore and aft asymmetry, decreases from about 35% to 15% of the isotropic term. The ratio of the $\cos^2\ \theta'$ term to the isotropic term does not change very much from an average value of about -0.4 in this energy region. This is equivalent to saying that the $\sin^2\ \theta'$ component of the angular distribution is roughly equal to 2/3 of the isotropic component, as can be seen by writing the expression for the angular distribution in the form

$$d\sigma/d\Omega' = 1 + C/A + (B/A)\ \cos\ \theta' - (C/A)\ \sin^2\ \theta'.$$

The Cal Tech data indicate a slight increase in the $\sin^2\ \theta'$ toward the upper end of this region.

The total cross sections obtained in this experiment are about 15% higher than the average of cross sections obtained elsewhere. The discrepancy is possibly due to the uncertainties in beam calibration, as discussed in Section IV-D. This explanation is supported by the fact that the 49^{o} cross sections obtained in the first and second synchrotron runs agreed quite well even though the experimental arrangements differed somewhat. If we use the calibration value of 4.00×10^{18} Mev/coulomb deduced in Section IV-D from the Cal Tech measurements, the discrepancy in total cross sections is reduced to about 8%. This experiment shows some indication of a drop in total cross section between 253 and 293 Mev.

C. Conclusions

Although there is no satisfactory explanation for the observed cross sections at high energies, some insight into the possible mechanisms involved may be gained by considering a few of the proposed theories.

The peak in the angular distribution in the vicinity of 90^{o} can be explained as the $\sin^{2}\theta'$ contribution produced by the electric dipole transition. The low-energy theories[3, 4, 5] predict this shape, and a predominantly $\sin^{2}\theta'$ angular distribution is obtained by Marshall and Guth[6] and by Schiff[7] in the energy region up to 150 Mev. In their calculations these authors used central forces and made various assumptions as to the shape, range, and exchange nature of the interaction between the neutron and proton. Only electric dipole and electric and magnetic quadrupole terms were considered. No explicit reference was made to meson theories. The calculations showed a forward shifting of the peak of the angular distribution as the energy is increased. This results from an interference between the electric dipole and electric quadrupole interactions. The magnetic quadrupole

interaction is the only one that gives a contribution at 0° and 180°, and its magnitude is very small compared to the electric dipole contribution.

Experiments up to 20 Mev reveal an almost pure $\sin^2 \theta'$ angular distribution, and this shape with a forward shift of the peak predominates up to 65 Mev in the work of Allen and Hanson[24] at Illinois. An isotropic component not predicted by the above theories is found by Allen and Hanson and also by Whalin[25] in an experiment extending from 60 to 165 Mev. The isotropic term extends up through the energy region of this experiment. The theories of Marshall and Guth and of Shiff seem to account fairly well for the decreasing $\sin^2 \theta'$ component, but not for the isotropic component. Austern,[29] in a calculation extending up to 100 Mev, showed that an isotropic component can arise from a noncentral force such as the singular $\vec{L}\cdot\vec{S}$ force used by Case and Pais[30] in their treatment of nucleon-nucleon scattering. Austern states that the force must be highly singular to produce the isotropic component.

The fact that the isotropic component of the cross section becomes important as the photomeson production threshold is approached suggests an explanation in terms of meson theories. The lack of a distinct change in the magnitude of the isotropic component in the vicinity of the meson threshold indicates some process that does not compete with the low-energy photomeson production. Such a process has been suggested by Wilson.[31] He assumes that if a meson is produced by a photon when the nucleons in the deuteron are within a radius of $\hbar/\mu c$, then the meson and two nucleons interact so strongly that they come into equilibrium before any particles are emitted. Under such conditions the statistical weights favor the reabsorption of the meson by one of the nucleons and the emission of two nucleons. The probability of emission of the meson is 10 percent or smaller. If the photon interacts with one of the nucleons when the nucleon

separation is somewhat larger than $\hbar/\mu c$, then meson emission is more probable than reabsorption. By use of the Hulthen wave function it is found that the nucleons are within a radius of $\hbar/\mu c$ about 20 percent of the time. The calculated ratio of photomeson cross section to photodisintegration cross section at 250 Mev is 3.6 as compared with an observed ratio of about 7.[32]

A possible explanation of the isotropic angular distribution of the meson contribution to the cross section may be found in an attempt to analyze the electric dipole transitions as those from the ^3S state to separate ^3P states. The ^3P_o state is isotropic whereas the $^3P_1$ and $^3P_2$ are not.[34] Thus an isotropic component near the π-meson threshold might arise from a process that favors transitions to the ^3P_o state. The work of Chew[33] suggests a meson reabsorption model leading to this final state. It is assumed that the photon interacts with one of the nucleons in the deuteron, flipping its spin and producing a meson in an S state. The subsequent reabsorption of the meson accoring to the Wilson[31] model would then lead to an odd-parity state with J = o, or to a ^3P_o state.

At energies corresponding to the I = 3/2, J = 3/2 resonance in the pion-nucleon system one expects an increase in the deuteron photodisintegration cross section because of the increase in photon absorption. Using this isobar model, Austern[35] has calculated an angular distribution of the form $1 + 3/2 \sin^2 \theta'$ and a cross section having a magnitude in rough agreement with the earlier data. He used as input data the $\pi^+ + D$ capture cross section, the $\pi + P$ scattering cross sections, and the $\gamma + P \rightarrow \pi^o + P$ cross section. Hanson[34] has reported a discussion by Feld in which the magnitude of the cross section was given as

$$\sigma_{D(\gamma, P)} \approx \sigma_{D(\gamma, \pi^o)} \frac{\sigma_{D(\pi^+, 2P)}}{\sigma_{D(\pi^+, \pi^+)}} \approx 240\ \mu b \frac{11\ mb}{121\ mb} \approx 22\ \mu b.$$

This is considerably less than the total cross section of about 65μb that is observed in the vicinity of 250 Mev, and it is stated that the calculated cross section would still be too low even if one included the total photon absorption cross section of about 400 μb instead of the π^o cross section as that leading to the resonant state. The data show a suggestion of the resonance with an angular distribution something like that indicated above.

Although the above considerations are helpful in understanding some of the features of deuteron photodisintegration in the high-energy region, no definite conclusions can be drawn concerning the exact nature of the interactions involved.

D. Extensions of the Experiment

Several possibilities have been suggested for improving the accuracy and completeness of the data. Perhaps the most obvious extension of the experiment is to continue operating with the existing apparatus to reduce the statistical errors. With reasonable effort, errors on the differential cross sections could probably be reduced to ± 5%. Cross sections at an additional angle in the vicinity of 160^o could be obtained without modification of the existing equipment. If a thinner dE/dx counter were used here and at 141^o, cross sections down to a photon energy of 136 Mev could be obtained. To obtain reliable results in the lower-energy channels at 36^o, it would be necessary to operate at a reduced beam energy. If counting errors in the deuteron photodisintegration cross sections were reduced to something like ± 5%, it would probably be desirable to make more accurate measurements on the nuclear attenuation in the counter telescope.

Experience with the present counter has suggested the desirability of improving the uniformity of light collection from the range counters. This would allow one to make better use of the pulse heights from these

counters in identifying particles. This would presumably make appreciable improvement in the separation of protons from background at the forward angles. If a new counter were constructed, its solid angle could be increased to several times its present value by using a rectangular aperture with its long dimension vertical rather than the present circular aperture.

No results have yet been published on high-energy deuteron photodisintegration for laboratory angles of less than about 30°. If a magnet were used, it should be possible to deflect the protons away from the beam and reduce the electron background so that results could be obtained at small angles , including 0°. One could also measure cross sections at 180° if desired. Although cross sections at these angles do not contribute appreciably to the total cross sections, they are desirable for a more precise knowledge of the angular distribution for the process.

In future work a pair counter will probably be used in addition to the other monitors to try to establish more precisely the absolute value of the cross sections.

ACKNOWLEDGMENTS

I wish to express my gratitude to Professor Burton J. Moyer for his encouragement and guidance throughout the experiment. Dr. Kenneth C. Bandtel has cooperated in all phases of the work and his assistance is appreciated. I am indebted to Mr. N. Fredrick Wikner and to other members of Professor Moyer's group for their assistance in the synchrotron runs and in reading and plotting the data. I wish to thank Mr. George McFarland and the synchrotron crew for their help in making the bombardments.

This work was performed under the auspices of the Atomic Energy Commission.

APPENDIX

A. Dynamics of Deuteron Photodisintegration

The proton kinetic energy as a function of photon energy and laboratory angle can be obtained by use of the expressions for the relativistic transformation of energy and momentum:

$$cp_x = \gamma cp'_x + \beta\gamma E', \tag{1}$$

$$cp_y = cp'_y, \tag{2}$$

$$cp_z = cp'_z, \tag{3}$$

$$E = \beta\gamma cp'_x + \gamma E'. \tag{4}$$

Here p_x, p_y, and p_z are components of momentum in the laboratory system, and E is the total energy in the laboratory. The primed quantities are the corresponding ones for the center-of-mass system; $c\beta$ is the velocity of the center-of-mass system with respect to the laboratory system; also $\gamma = (1 - \beta^2)^{-1/2}$. (5)

We can obtain the β of the center-of-mass system by applying Eq. (1) and (4) to the γ + d system before the collision.

$$E_\gamma = 0 + \beta\gamma(E'_\gamma + E_o), \tag{6}$$

$$E_\gamma + M_d c^2 = 0 + \gamma(E'_\gamma + E_o). \tag{7}$$

From Eqs. (5), (6), and (7),

$$\beta = E_\gamma/(E_\gamma + M_d c^2)$$

and $$\gamma = (E_\gamma + M_d c^2)/(2E_\gamma M_d c^2 + M_d^2 c^4)^{1/2}. \tag{8}$$

The total laboratory energy of a proton leaving the target at a laboratory angle θ can be obtained by applying Eq. (4) to the proton and using the expressions $cp'_x = cp'\cos\theta$ and $E_p^2 = c^2 p'^2 + M_p^2 c^4$. Here p' is the center-of-mass momentum of the proton. The result is

$$E_p = \beta\gamma\cos\theta'(E'^2_p - M_p^2 c^4)^{1/2} + \gamma E'_p. \tag{9}$$

We need to express E'_p in terms of known quantities. Equation (4) applied to the γ + d system gives

$$E' = E/\gamma = (E_\gamma + M_d c^2)/\gamma. \tag{10}$$

The total center-of-mass energy after the collision is the same as that before, so

$$E' = E'_p + E'_n \tilde{=} 2E'_p \tag{11}$$

where E'_n is the total neutron energy. From Eqs. (8), (10), and (11),

$$E'_p = (E_\gamma + M_d c^2)/2\gamma = 1/2(2E_\gamma M_d c^2 + M_d^2 c^4)^{1/2}. \tag{12}$$

To simplify matters we can express the deuteron rest energy in terms of the proton rest energy by considering the neutron-proton mass difference and deuteron binding energy.

$$\begin{aligned} M_d c^2 &= M_p c^2 + M_n c^2 - \text{B.E.} \\ &= 2M_p c^2 + (M_n c^2 - M_p c^2) - \text{B.E.} \\ &= 2M_p c^2 - b \tilde{=} 2M_p c^2 - 1 \text{ Mev.} \end{aligned} \tag{13}$$

The proton kinetic energy is $T_p = E_p - M_p c^2$, so by using Eqs. (9), (12), and (13) and neglecting some small terms involving b we get the approximate expression

$$T_p = (E - b)/2 + \frac{E_\gamma}{2} \cos\theta' \frac{E_\gamma}{(E_\gamma + M_p c^2)^{1/2}}.$$

Cross sections are measured in the laboratory system, and we desire to transform them to center-of-mass cross sections. We therefore need expressions to transform angles and solid angles. Consider a proton leaving the target at a laboratory angle θ. Using Eqs. (1) and (2) we can obtain

$$\tan\theta = \frac{cp_y}{cp_x} = \frac{cp'_y}{\gamma cp'_x + \beta\gamma E'_p} = \frac{1}{\gamma\cot\theta' + \beta\gamma E'_p / \sin\theta' \sqrt{E'^2_p - M_p^2 c^4}},$$

which gives the desired relation between laboratory and center-of-mass angles. The above equation may be differentiated to give

$$\frac{d\theta}{d\theta'} = \gamma \frac{\sin^2\theta}{\sin^2\theta'} \left[1 + \frac{\beta E'_p \cos\theta'}{(E'^2_p - M_p^2 c^4)^{1/2}} \right].$$

Then the ratio between laboratory solid angle and center-of-mass solid angle is

$$\frac{d\Omega}{d\Omega'} = \frac{2\pi \sin\theta d\theta}{2\pi \sin\theta' d\theta'} = \frac{\gamma \sin^3\theta}{\sin^3\theta'}\left[1 - \frac{\beta E_p'}{(E_p'^2 - M_p^2 c^4)^{1/2}}\right].$$

B. Curve Fitting

For a given energy, differential cross sections, $\sigma_m(\theta_i')$, were measured at various angles. The subscript m indicates measured cross section. It was desired to fit a curve of the form

$$\sigma(\theta') = A + B\cos\theta' + C\cos^2\theta'.$$

The criterion for a best fit is that

$$f \equiv W_i V_i^2 = \text{minimum.}$$

Here $V_i = A + B\cos\theta_i' + C\cos^2\theta_i' - \sigma_m(\theta_i')$, and

$W_i = 1/(\text{standard deviation of } \sigma_m(\theta_i'))^2$.

We minimize f by setting

$$\partial f/\partial A = 0,\ \partial f/\partial B = 0,\ \partial f/\partial C = 0.$$

This leads to the following set of equations:

$$A\Sigma W_i + B\Sigma W_i \cos\theta_i' + C\Sigma W_i \cos^2\theta_i' = \Sigma W_i \sigma_m(\theta_i'),$$

$$A\Sigma W_i \cos\theta_i' + B\Sigma W_i \cos^2\theta_i' + C\Sigma W_i \cos^3\theta_i' = \Sigma W_i \cos\theta_i' \sigma_m(\theta_i'),$$

$$A\Sigma W_i \cos^2\theta_i' + B\Sigma W_i \cos^3\theta_i' + C\Sigma W_i \cos^4\theta_i' = \Sigma W_i \cos^2\theta_i' \sigma_m(\theta_i').$$

These are solved for A, B, and C by use of determinants.

To obtain errors on A, B, and C we define the "standard deviation for an observation of unit weight,"

$$\Delta_{\sigma(\theta_i')} = \sqrt{\frac{\Sigma W_i \left[\sigma(\theta_i') - \sigma_m(\theta_i')\right]^2}{n-q}},$$

where q is the number of unknown independent parameters (there are three) and n is the number of observations. Then the standard deviations in A, B, and C are

$$\Delta_A = \Delta_{\sigma(\theta_i')} \sqrt{\frac{A_{11}}{D}} ,$$

$$\Delta_B = \Delta_{\sigma(\theta_i')} \sqrt{\frac{A_{22}}{D}} ,$$

$$\Delta_C = \Delta_{\sigma(\theta_i')} \sqrt{\frac{A_{33}}{D}} .$$

Here D is the determinant formed from the coefficients of A, B, and C in the above set of equations. A_{11} is the determinant formed by eliminating the first row and first column from D and similarly for A_{22} and A_{33}.

REFERENCES

1. J. Chadwick and M. Goldhaber, Proc. Roy. Soc. (London) A151, 479 (1935).
2. H. A. Bethe and R. Peierls, Proc. Roy. Soc. (London) A148, 146 (1935).
3. N. F. Ramsey in E. Segre, Experimental Nuclear Physics(John Wiley and Sons, New York, 1953), Vol. 1.
4. G. L. Squires in O. R. Frisch, Progress in Nuclear Physics (Academic Press, Inc., New York, 1952), Vol. 2.
5. J. M. Blatt and V. F. Weidkopf, Theoretical Nuclear Physics (John Wiley and Sons, New York, 1952).
6. J. F. Marshall and E. Guth, Phys. Rev. 78, 738 (1950).
7. L. I. Schiff, Phys. Rev. 78, 733 (1950).
8. T. S. Benedict and W. M. Woodward, Phys. Rev. 85, 924 (1952).
9. S. Kikuchi, Phys. Rev. 85, 1062 (1952).
10. R. Littauer and J. C. Keck, Phys. Rev. 86, 1051 (1952).
11. W. Gilbert and J. W. Rosengren, Phys. Rev. 88, 901 (1952).
12. J. D. Anderson, R. W. Kenney, and C. A. McDonald, private communication.
13. R. Madey, "The Photoproduction of Negative Pions from Deuterium," (Thesis) University of California Radiation Laboratory Report No. UCRL-1634, January 1952.
14. W. M. Powell, W. Hartsough, and M. Hill, Phys. Rev. 81,213 (1951).
15. L. H. Lanzl and A. O. Hanson, Phys. Rev. 83, 959 (1951).
16. B. Rossi, High-Energy Particles (Prentice-Hall, New York, 1952).
17. R. Madey, "A Fast Counting System for High-Energy Particle Measurements," University of California Radiation Laboratory Report No. 1880 (1954).

18. T. Yamogata, M. Q. Barton, A. O. Hanson, and J. H. Smith, Phys. Rev. 95, 574 (1954).
19. O. Chamberlain, E. Segre, and C. Wiegand, Phys. Rev. 83,923 (1951).
20. J. Hadley, E. Kelley, C. Leith, E. Segrè, C. Wiegand, and H. York, Phys. Rev. 75, 351 (1949).
21. H. W. Woolley, R. B. Scott, and F. G. Brickwedde, J. Research Natl. Bur. Standards 41, 379 (1948).
22. W. Blocker, R. W. Kenney, and W. K. H. Panofsky, Phys. Rev. 79, 419 (1950).
23. J. Keck, R. M. Littauer, G. K. O'Neill, A. M. Perry, and W. M. Woodward, Phys. Rev. 93, 827 (1954).
24. L. Allen, Jr., and A. O. Hanson, Phys. Rev. 95, 629 (1954).
25. E. A. Whalin, Jr., Phys. Rev. 95, 1362 (1954).
26. J. D. Anderson, R. W. Kenney, and C. A. McDonald, Bull. Am. Phys. Soc. 29, No. 8 (1954), and private communication.
27. B. D. Schriever, E. A. Whalin, and A. O. Hanson, Phys. Rev. 94, 763 (1954).
28. A. V. Tollestrup, J. C. Keck, and W. R. Smythe II, Bull. Am. Phys. Soc. 29, No. 6, p. 15 (1954).
29. N. Austern, Phys. Rev. 85, 283 (1952).
30. K. M. Case and A. Pais, Phys. Rev. 80, 203 (1950).
31. R. R. Wilson, Phys. Rev. 86, 125 (1952).
32. E. A. Whalin, Jr., "Photodisintegration of Deuterons by 165-Mev X-Rays (Thesis), University of Illinois, (1954). Unpublished.
33. G. F. Chew, Phys. Rev. 95, 1669 (1954).
34. A. O. Hanson, invited paper, Bull. Am. Phys. Soc. 29, No. 7, p. 19 (1954), and private communication thereon.
35. N. Austern, Phys. Rev. 87, 208 (1952).
36. R. L. Walker, J. G. Teasdale, V. Z. Peterson, J. I. Vette, Photoproduction of Positive Pions in Hydrogen–Magnetic Spectrometer Method, (to be published).